From weak lensing to non-Gaussianity via Minkowski functionals

Article (Published Version)

Monthly Notices
of the
ROYAL ASTRONOMICAL SOCIETY

Mon. Not. R. Astron. Soc. **419,** 536–555 (2012) doi:10.1111/j.1365-2966.2011.19718.x

From weak lensing to non-Gaussianity via Minkowski functionals

Dipak Munshi,[1⋆] Ludovic van Waerbeke,[2] Joseph Smidt[3] and Peter Coles[1]

[1]*School of Physics and Astronomy, Cardiff University, Queens Buildings, 5 The Parade, Cardiff CF24 3AA*
[2]*Department of Physics & Astronomy, University of British Columbia, 6224 Agricultural Road, Vancouver, BC V6T 1Z1, Canada*
[3]*Department of Physics and Astronomy, University of California, Irvine, CA 92697, USA*

Accepted 2011 August 26. Received 2011 June 21; in original form 2011 March 15

ABSTRACT

We present a new harmonic-domain-based approach for extracting morphological information, in the form of Minkowski functionals (MFs), from weak-lensing convergence maps. Using a perturbative expansion of the MFs, which is expected to be valid for the range of angular scales probed by most current weak-lensing surveys, we show that the study of three generalized skewness parameters is equivalent to the study of the three MFs defined in 2D. We then extend these skewness parameters to three associated skew spectra which carry more information about the convergence bispectrum than their one-point counterparts. We discuss various issues such as noise and incomplete sky coverage in the context of estimation of these skew spectra from realistic data. Our technique provides an alternative to the pixel-space approaches typically used in the estimation of MFs, and it can be particularly useful in the presence of masks with non-trivial topology. Analytical modelling of weak-lensing statistics relies on an accurate modelling of the statistics of the underlying density distribution. We apply three different formalisms to model the underlying dark matter bispectrum: the hierarchical ansatz, halo model and a fitting function based on numerical simulations; MFs resulting from each of these formalisms are computed and compared. We investigate the extent to which late-time gravity-induced non-Gaussianity (to which weak lensing is primarily sensitive) can be separated from primordial non-Gaussianity and how this separation depends on source redshift and angular scale.

Key words: gravitational lensing: weak – methods: analytical – methods: numerical – methods: statistical – cosmology: theory – large-scale structure of Universe.

1 INTRODUCTION

Since the first measurements were published (Beacon, Refregier & Ellis 2000; Kaiser, Wilson & Luppino 2000; Van Waerbeke et al. 2000; Wittman et al. 2000), there has been tremendous progress in the field of weak gravitational lensing, regarding analytical modelling as well as technical specification and control of systematics in observational surveys. Ongoing and planned weak-lensing surveys (see Munshi et al. 2008 for a review) such as the CFHT[1] Legacy Survey, Pan-STARRS,[2] the Dark Energy Survey,[3] and, further in the future, the Large Synoptic Survey Telescope,[4] JDEM[5] and *Euclid*[6] will map the cosmological distribution of dark matter and probe the properties of dark energy in unprecedented detail. Owing to the greater sky coverage, tighter control on systematics and increased number density of source galaxies, it will be soon possible to extract higher order statistics (i.e. beyond the two-point correlation function), such as multispectra (see e.g. Pen et al. 2003). Non-linearity induced by gravitational effects is generally used to break the degeneracy between the amplitude of matter power spectrum σ_8 and the matter density parameter $\Omega_{\rm M}$; three-point statistics such as the bispectrum (the three-point multispectrum) are the best studied statistics for this purpose (Villumsen 1996; Jain & Seljak 1997). Weak lensing can therefore play an important role in breaking

⋆E-mail: Dipak.Munshi@astro.cf.ac.uk
[1] http://www.cfht.hawai.edu/Sciences/CFHLS/
[2] http://pan-starrs.ifa.hawai.edu/
[3] http://www.darkenergysurvey.org/
[4] http://www.lsst.org/llst_home.shtml
[5] http://jdem.gsfc.nasa.gov/
[6] http://sci.esa.int/euclid

degeneracies, which makes it an ideal complement to cosmic microwave background (CMB) studies and studies involving large-scale structure (LSS) surveys.

Two-point statistics, principally the power spectrum, of density perturbations remain the most frequently used statistical tool for many cosmological studies. Weak-lensing surveys probe the non-linear regime and are therefore sensitive to non-Gaussian signatures which cannot be probed using two-point statistics. The statistics of shear or convergence probe the statistics of underlying mass distribution in an unbiased way (Jain, Seljak & White 2000; Munshi 2000; Munshi & Jain 2000, 2001; Valageas 2000; Takada & Jain 2004; Takada & White 2004; Valageas, Barber & Munshi 2004; Munshi & Valageas 2005; Valageas, Munshi & Barber 2005), but are very sensitive to non-linear evolution driven by gravitational clustering. A number of analytical schemes, from perturbative calculations to halo models, have therefore been employed to model weak-lensing statistics (Fry 1984; Schaeffer 1984; Bernardeau & Schaeffer 1992; Szapudi & Szalay 1993, 1997; Munshi et al. 1999a, 2011a; Munshi, Coles & Melott 1999b,c; Munshi, Melott & Coles 1999d; Munshi & Coles 2000, 2002, 2003; Cooray & Seth 2002; Munshi, Valageas & Barber 2004). In addition to studying the statistics in projection on the sky, they have also been studied in 3D using photometric redshifts. It has been demonstrated that this approach can tighten observational constraints on such quantities as the neutrino mass and the dark energy equation-of-state parameter (Heavens, Refregier & Heymans 2000; Heavens 2003; Castro, Heavens & Kitching 2005; Heavens, Kitching & Taylor 2006; Heavens, Kitching & Verde 2007; Kitching et al. 2008). Tomographic techniques have also been employed as an intermediate strategy between projected surveys and 3D mapping (Hu 1999; Takada & Jain 2003, 2004; Semboloni et al. 2008). Minkowski functionals (MFs) are morphological descriptors that are commonly used in many cosmological contexts. They can be defined for both 2D (projected) and 3D (redshift) data, and have been used to probe non-Gaussianity in CMB data (Komatsu et al. 2003; Eriksen et al. 2004; Hikage et al. 2008b; Natoli et al. 2010), weak-lensing surveys (Matsubara & Jain 2001; Sato et al. 2001; Taruya et al. 2002) and galaxy surveys (Gott, Melott & Dickinson 1986; Coles 1988; Gott et al. 1989, 1992; Melott 1990; Moore et al. 1992; Rhodas, Gott & Postman 1994; Canavezes et al. 1998; Hikage et al. 2002, 2008a; Hikage, Taruya & Suto 2003; Park et al. 2005; Hikage, Komatsu & Matsubara 2006). Unlike the multispectra discussed above, the topological descriptors carry information of all orders (in a statistical sense). In the context of CMB studies, the MFs are used to probe primordial non-Gaussianity. For LSS studies using projected or redshift galaxy surveys, the non-Gaussianity probed is mainly that which is induced by gravity. While galaxy surveys suffer from uncertainties relating to the nature of galaxy bias, weak-lensing surveys will provide an unbiased probe to probe the clustering of dark matter. The MFs will be an important tool in this direction, along with other statistics that can be used to probe non-Gaussianity to break the parameter space, which are unavoidable when the power spectrum alone is used.

This paper is organized as follows. In Section 2, we review the formalism of MF. In Section 3, we link the statistics of weak-lensing convergence and the underlying density distribution. In Section 4, we introduce the concept of generalized skew spectra and show how these power spectra can be used to study the MFs. In Section 5, we review the analytical models that are typically used for modelling of dark matter clustering.

2 FORMALISM

The MFs are well-known morphological descriptors that are used in the study of random fluctuation fields. Morphological properties are defined to be those properties that remain invariant under rotation and translation (see Hadwiger 1959 for a more formal introduction). They are defined over an excursion set Σ for a given threshold ν. The three MFs that are defined for 2D studies can be expressed, following the notations of Hikage et al. (2008a), as

$$V_0(\nu) = \int_\Sigma \mathrm{d}a; \quad V_1(\nu) = \frac{1}{4}\int_{\partial\Sigma} \mathrm{d}l; \quad V_2(\nu) = \frac{1}{2\pi}\int_{\partial\Sigma} \mathcal{K}\,\mathrm{d}l. \tag{1}$$

Here da and dl are the surface and line element for the excursion set Σ and its boundary $\partial\Sigma$, respectively. The MFs $V_k(\nu)$ correspond to the area of the excursion set Σ, the length of its boundary $\partial\Sigma$ as well as the integral of curvature $\mathcal{K}$ along its boundary which is also related to the genus g and hence the Euler characteristics χ.

In our analysis, we will consider a smoothed random field $\kappa(\hat{\mathbf{\Omega}})$, with mean $\langle\kappa(\hat{\mathbf{\Omega}})\rangle = 0$ and variance $\sigma_0^2 = \langle\kappa^2(\hat{\mathbf{\Omega}})\rangle$; for the time being, κ is a generic 2D weakly non-Gaussian random field defined on the sky, although we will introduce more specific examples later on. The spherical harmonic decomposition, using $Y_{lm}(\hat{\mathbf{\Omega}})$ as basis functions, $\kappa(\hat{\mathbf{\Omega}}) = \sum_{lm}\kappa_{lm}Y_{lm}(\hat{\mathbf{\Omega}})$, can be used to define the power spectrum $\mathcal{C}_l$ using $\langle\kappa_{lm}\kappa^*_{l'm'}\rangle = \mathcal{C}_l\delta_{ll'}\delta_{mm'}$ which is a sufficient statistical characterization of a Gaussian field. In Fig. 1 (left-hand panel), we plot the angular power spectra $\mathcal{C}_l$ for the 7-year *Wilkinson Microwave Anisotropy Probe* (*WMAP*7) background cosmology. Three different redshifts are chosen, $z_s = 0.5$, 1.0 and 1.5. We show two different theoretical models: perturbation theory (PT) and halo model. For a non-Gaussian field, higher order statistics such as the bi- or tri-spectrum can describe the resulting mode–mode coupling. The right-hand panel of Fig. 1 also shows the diagonal terms of the bispectrum for PT and halo model. An alternative to this laborious expansion in multispectra, topological measures such as the MFs can be employed to quantify deviations from Gaussianity and it can be shown that the content in both descriptions is the same. At leading order, the MFs can be constructed completely from the knowledge of the bispectrum alone. We will be studying the MFs defined over the surface of the celestial sphere, but equivalent results can be obtained in 3D using Fourier decomposition (Munshi, in preparation). The behaviour of the MFs for a random Gaussian field is well known and is given by Tomita's formula (Tomita 1986). The MFs are denoted by $V_k(\nu)$ for a threshold $\nu = \kappa/\sigma_0$, where $\sigma_0^2 = \langle\kappa^2\rangle$ can be decomposed into two different contributions, Gaussian $[V_k^{\rm G}(\nu)]$ and non-Gaussian $[\delta V_k(\nu)]$, that is, $V_k(\nu) = V_k^{\rm G}(\nu) + \delta V_k(\nu)$. From our perspective, we will be more interested in the non-Gaussian contribution, that is, $\delta V_k(\nu)$. We will further separate out an amplitude A in the expressions of both these contributions which depend only on the power

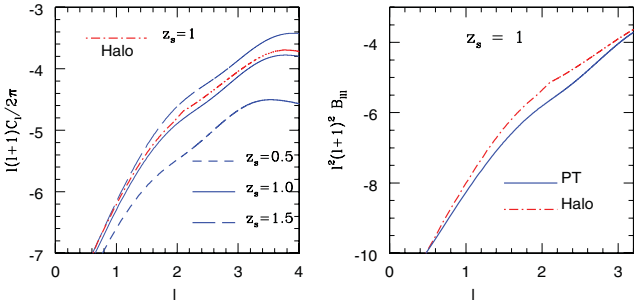

Figure 1. The power spectrum is plotted as a function of the harmonics l in the left-hand panel. A *WMAP*7 background cosmology is used. The results are displayed for three different source redshifts $z_s = 1.5$, 1.0 and 0.5. The cosmological parameters are $\Gamma = 0.1956$, $\Omega_M = 0.279$, $\Lambda = 0.721$ and $\sigma_8 = 0.817$. The dot–dashed curve shows predictions from the halo model for the same *WMAP*7 background cosmology and for the source redshift $z_s = 1$. The diagonal entries of the bispectrum are plotted as a function of the harmonics l in the right-hand panel. The results are for $z_s = 1.0$. Two different approaches are persued in the computation of the bispectrum. The bispectrum results based on extensions of PT (equation 34) are plotted using the solid lines and the halo model predictions, that is, equation (31), are shown using the dashed lines.

spectrum of the perturbation through $\sigma_0 = \langle\kappa^2\rangle^{1/2}$ and $\sigma_1 = \langle(\nabla\kappa)^2\rangle^{1/2}$ (see e.g. Hikage et al. 2008a):

$$V_k^{\rm G}(\nu) = A\exp\left(-\frac{\nu^2}{2}\right)H_{k-1}; \qquad \delta V_k(\nu) = A\exp\left(-\frac{\nu^2}{2}\right)\left[\delta V_k^{(2)}(\nu)\sigma_0 + \delta V_k^{(3)}(\nu)\sigma_0^2 + \delta V_k^{(4)}(\nu)\sigma_0^3 + \cdots\right]; \tag{2}$$

$$\delta V_k^{(2)}(\nu) = \left\{\left[\frac{1}{6}S^{(0)}H_{k+2}(\nu) + \frac{k}{3}S^{(1)}H_k(\nu) + \frac{k(k-1)}{6}S^{(2)}H_{k-2}(\nu)\right]\right\}; \qquad A = \frac{1}{(2\pi)^{(k+1)/2}}\frac{\omega_2}{\omega_{2-k}\omega_k}\left(\frac{\sigma_1}{\sqrt{2}\sigma_0}\right)^k. \tag{3}$$

The constant ω_k introduced above is the volume of the unit sphere in k dimensions, that is, $w_k = \pi^{k/2}/\Gamma(k/2+1)$; in 2D, we need only $\omega_0 = 1$, $\omega_1 = 2$ and $\omega_2 = \pi$. The lowest order Hermite polynomials $H_k(\nu)$ are listed below. As mentioned previously, the expressions consist of two distinct contributions. The part which does not depend on the three different skewness parameters, $S^{(0)}$, $S^{(1)}$ and $S^{(2)}$, signifies the MFs for a Gaussian random field. The other contribution $\delta V_k(\nu)$ represents the departure from the Gaussian statistics and depends on the generalized skewness parameters defined in equations (5) and (9). We have expanded the total non-Gaussian contribution into perturbation series in σ_0. While the lowest order terms $\delta V_k^{(2)}(\nu)$ are determined by various one-point moments related to the bispectrum, the next-to-leading-order terms $\delta V_k^{(3)}(\nu)$ are connected to similar one-point moments related to the trispectrum (also known as the kurtosis). In projected surveys, even for relatively small angular smoothing scales, the leading-order terms are sufficient to describe the non-Gaussian departures in the smoothed convergence field $\kappa(\theta_s)$ (see e.g. Hikage et al. 2008a). The Hermite polynomials $H_n(\nu)$ and their generating functions are given below:

$$H_{-1}(\nu) = \sqrt{\frac{\pi}{2}}e^{\nu^2/2}{\rm erfc}\left(\frac{\nu}{\sqrt{2}}\right); \quad H_0(\nu) = 1; \quad H_1(\nu) = \nu;$$
$$H_2(\nu) = \nu^2 - 1; \quad H_3(\nu) = \nu^3 - 3\nu; \qquad H_4(\nu) = \nu^4 - 6\nu^2 + 3;$$
$$H_n(\nu) = (-1)^n\exp\left(\frac{\nu^2}{2}\right)\frac{{\rm d}}{{\rm d}\nu^n}\exp\left(\frac{-\nu^2}{2}\right). \tag{4}$$

The lower order Hermite polynomials are plotted in Fig. 2. The various quantities σ_j that appear in equation (3) can be expressed in terms of the power spectra C_l and the shape of the observational beam b_l. The moment σ_0 is a special case for which σ_0^2 corresponds to the variance. The

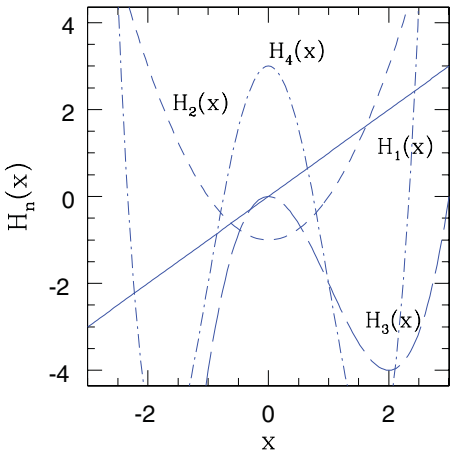

Figure 2. The Hermite polynomials that are used as a basis function for expanding the MF in the weakly non-Gaussian limit. The plots show $H_1(x)$ (solid line), $H_2(x)$ (short-dashed line), $H_3(x)$ (long-dashed line) and $H_4(x)$ (dot–dashed line) as a function of the argument x as depicted.

quantities σ_1 and σ_2 are natural generalizations of variance, with increasing j corresponding to increase in weight towards higher harmonics $\sigma_j^2 = \frac{1}{4\pi}\sum(2l+1)[l(l+1)]^j \mathcal{C}_l b_l^2$. The variances that will be used mostly are $\sigma_0^2 = \langle\kappa^2\rangle$ and $\sigma_1^2 = \langle(\nabla\kappa)^2\rangle$.

The real-space expressions for the triplets of skewness $S^{(i)}$ are given below. These are natural generalizations of the ordinary skewness S^0 that is used in many cosmological studies. They all are cubic statistics but are constructed from different cubic combinations:

$$S^{(0)} \equiv \frac{S^{(\kappa^3)}}{\sigma_0^4} = \frac{\langle\kappa^3\rangle}{\sigma_0^4}; \quad S^{(1)} \equiv -\frac{3}{4}\frac{S^{(\kappa^2,\nabla^2\kappa)}}{\sigma_0^2} = -\frac{3}{4}\frac{\langle\kappa^2\nabla^2\kappa\rangle}{\sigma_0^2\sigma_1^2}; \quad S^{(2)} \equiv S^{(\nabla\kappa\cdot\nabla\kappa,\nabla^2\kappa)} = -3\frac{\langle(\nabla\kappa)\cdot(\nabla\kappa)(\nabla^2\kappa)\rangle}{\sigma_1^4}. \tag{5}$$

The expressions in the harmonic domain are more useful in the context of CMB studies where we will be recovering them from a masked sky using analytical tools that are commonly used for power spectrum analysis. The skewness parameter $S^{(1)}$ is constructed from the product field κ^2 and $\nabla^2 f$, whereas the skewness parameter $S^{(2)}$ relies on the construction of $(\nabla\kappa\cdot\nabla\kappa)$ and $\nabla^2\kappa$. By construction, the skewness parameter $S^{(2)}$ has the highest weight at high-l modes and $S^{(0)}$ has the lowest weights on high-l modes. The expressions in terms of the bispectrum $B_{l_1l_2l_3}$ (see equation 10 for definition) take the following forms (see e.g. Hikage et al. 2008a):

$$S^{(\kappa^3)} = \frac{1}{4\pi}\sum_{l_i}\mathcal{B}_{l_1l_2l_3}I_{l_1l_2l_3}; \tag{6}$$

$$S^{(\kappa^2,\nabla^2\kappa)} = -\frac{1}{12\pi}\sum_{l_i}[l_1(l_1+1)+l_2(l_2+1)+l_3(l_3+1)]\mathcal{B}_{l_1l_2l_3}I_{l_1l_2l_3}; \tag{7}$$

$$S^{(\nabla\kappa\cdot\nabla\kappa,\nabla^2\kappa)} = \frac{1}{4\pi}\sum_{l_i}\Big\{[l_1(l_1+1)+l_2(l_2+1)-l_3(l_3+1)]l_3(l_3+1)+\text{cyclic permutation}\Big\}\mathcal{B}_{l_1l_2l_3}I_{l_1l_2l_3}W_{l_1}W_{l_2}W_{l_3}; \tag{8}$$

$$I_{l_1l_2l_3} = \sqrt{\frac{(2l_1+1)(2l_2+1)(2l_3+1)}{4\pi}}\begin{pmatrix} l_1 & l_2 & l_3 \\ 0 & 0 & 0\end{pmatrix}. \tag{9}$$

The bispectrum $B_{l_1l_2l_3}$ used here defines the three-point correlation function in the harmonic domain. A reduced bispectrum $b_{l_1l_2l_3}$ can also be defined which can directly be linked to the *flat-sky* expressions:

$$\langle\kappa_{l_1m_1}\kappa_{l_2m_2}\kappa_{l_3m_3}\rangle_{\rm c} = \begin{pmatrix} l_1 & l_2 & l_3 \\ m_1 & m_2 & m_3\end{pmatrix}\mathcal{B}_{l_1l_2l_3}; \qquad \mathcal{B}_{l_1l_2l_3} = I_{l_1l_2l_3}b_{l_1l_2l_3}. \tag{10}$$

The expressions for the MFs in equation (3) depend on the one-point cumulants $S^{(i)}$. However, it is possible to define power spectra associated with each of these skewnesses following a procedure developed in Munshi & Heavens (2010). This will mean we can also associate a power spectrum with $V_k^{(3)}$ which will generalize the concept of MFs in a scale-dependent way. The power spectrum that we associate with MFs will have the same correspondence with various skew spectra $S_l^{(i)}$ as the MFs have with one-point cumulants or $S^{(0)}$. The power spectra so defined will, however, have more power to distinguish between various models of non-Gaussianity. This is one of the main motivations behind generalizing the concept of MFs, each of which is a number, to a power spectrum, which contains scale information.

The series expansion for the MFs can be extended beyond the level of the bispectrum; the next-to-leading-order correction terms are related to trispectra of the original fields and various derivatives constructed from them using differential operations such as $\nabla\cdot\nabla$, ∇^2. These corrections are expected to be subdominant in the context of CMB studies for the entire range of angular scales being probed.

The results here correspond to analysis of convergence maps, which are spin-0 objects. It is possible to extend these results to spin-2 fields. Such results will be interesting for the analysis of weak-lensing shear and flexions, but a detailed analysis will be presented elsewhere.

3 CONVERGENCE POWER SPECTRUM AND BISPECTRUM

The convergence $\kappa(\hat{\mathbf{\Omega}}, r_{\rm s})$ can be treated as a line-of-sight projection of the density contrast $\delta(\hat{\mathbf{\Omega}}, r)$ along the direction $\hat{\mathbf{\Omega}}$ (r is a comoving radial distance) out to a source redshift $z_{\rm s}(r_{\rm s})$ with a redshift-dependent weight function $\omega(r, r_{\rm s})$:

$$\kappa(\hat{\mathbf{\Omega}}, r_{\rm s}) = \int_0^{r_{\rm s}} {\rm d}r\, w(r, r_{\rm s})\,\delta(\hat{\mathbf{\Omega}}, r); \quad \omega(r, r_{\rm s}) = \frac{3}{2a}\frac{H_0^2}{c^2}\Omega_{\rm M}\frac{d_{\rm A}(r-r_{\rm s})}{d_{\rm A}(r)d_{\rm A}(r_{\rm s})}; \quad r_{\rm s} = \min(r_1, r_2). \tag{11}$$

The weight functions $\omega(r)$ for weak lensing depend on the angular diameter distance $d_{\rm A}(r)$, Hubble constant H_0, matter density parameter $\Omega_{\rm M}$ and the scalefactor of the Universe $a = 1/(1+z)$ at a redshift z. The angular diameter distance $d_{\rm A}(r)$ is linked to the total matter content Ω_0 and the Hubble constant H_0, that is, $d_{\rm A}(r) = K^{-1/2}\sin(K^{-1/2}r), K^{-1/2}\sinh[(-K)^{-1/2}r]$ and r for open, closed and flat universes, respectively; here $K = (\Omega_0 - 1)H_0^2$. We will consider the projected cross-power spectra C_l that depend on two different redshifts z_1 and z_2 which are a function of the underlying matter power spectra $P_\delta(k, r)$ which, in the small-angle approximation (Limber 1954), can be expressed as (Kaiser 1992)

$$\mathcal{C}_l = \int_0^{r_{\rm s}} {\rm d}r\ \frac{w^2(r; r_{\rm s})}{d_{\rm A}^2(r)}P_{\rm nl}^{\delta}\left(\frac{l}{d_{\rm A}(r)}, r\right). \tag{12}$$

Analytical modelling of the convergence bispectrum $\mathcal{B}$ depends on the modelling of the underlying matter bispectrum B_δ:

$$\mathcal{B}_{l_1l_2l_3} = I_{l_1l_2l_3}\int_0^{r_{\rm s}} {\rm d}r\,\frac{w^3(r, r_{\rm d})}{d_{\rm A}^4(r)}B_{\rm nl}^{\delta}\left(\frac{l_1}{d_{\rm A}(r)}, \frac{l_2}{d_{\rm A}(r)}, \frac{l_3}{d_{\rm A}(r)}\right); \tag{13}$$

we will discuss the analytical models we used to construct B_δ in later sections. This equation can also be used to express the reduced bispectrum $b_{l_1 l_2 l_3}$ introduced before in equation (10). Estimation of individual modes of the bispectrum defined by a specific choice of the triplets (l_1, l_2, l_3) is difficult when the data are noisy, but it is possible to extract the cross-correlation of product maps $\kappa^2(\hat{\mathbf{\Omega}})$ against $\kappa(\hat{\mathbf{\Omega}})$. If we denote the harmonics of the product map $\kappa^2(\hat{\mathbf{\Omega}})$ as $\kappa^{(2)}_{lm} = \int A\hat{\mathbf{\Omega}}\, Y^*_{lm}(\hat{\mathbf{\Omega}})\kappa^2(\hat{\mathbf{\Omega}})$, and similarly $\kappa_{lm} = \int \mathrm{d}\hat{\mathbf{\Omega}}\, Y^*_{lm}(\hat{\mathbf{\Omega}})\kappa(\hat{\mathbf{\Omega}})$, then the associated power spectrum is constructed as $C^{(2,1)}_l = \frac{1}{2l+1}\sum_l \mathrm{Re}[\kappa^{(2)}_{lm}\kappa^{(1)}_{lm}]$ and is called the skew spectrum (Cooray 2001a). We will next generalize the concept of a skew spectrum and introduce a set of generalized skew spectra that can be used to construct the MFs at the lowest level of non-Gaussianity.

4 THE TRIPLETS OF SKEW SPECTRA AND LOWEST ORDER CORRECTIONS TO GAUSSIAN MINKOWSKI FUNCTIONALS

The skew spectra are cubic statistics that are constructed by cross-correlating two different fields. One of the fields used is a composite field, typically a product of two maps either in its original form or constructed by means of relevant differential operations. The second field will typically be a single field but may be constructed by applying various differential operators. All three skewnesses contribute to the three MFs that we will consider in 2D.

The first of the skew spectra was studied by Cooray (2001a) and was later generalized by Munshi & Heavens (2010) and is related to commonly used skewness. The skewness in this case is constructed by cross-correlating the squared map $[\kappa^2(\hat{\mathbf{\Omega}})]$ with the original map $[\kappa(\hat{\mathbf{\Omega}})]$. The second skew spectrum is constructed by cross-correlating the squared map $[\kappa^2(\hat{\mathbf{\Omega}})]$ against $[\nabla^2\kappa(\hat{\mathbf{\Omega}})]$. Analogously, the third skew spectrum represents the cross-spectra that can be constructed using $[\nabla\kappa(\hat{\mathbf{\Omega}})\cdot\nabla\kappa(\hat{\mathbf{\Omega}})]$ and $[\nabla^2\kappa(\hat{\mathbf{\Omega}})]$ maps. The skew spectra $S^{(0)}_l$, $S^{(0)}_l$ and $S^{(0)}_l$ can be expressed in terms of the convergence bispectrum $\mathcal{B}_{l_1 l_2 l_3}$ using the following expressions:

$$S^{(0)}_l \equiv \frac{1}{12\pi\sigma_0^4} S^{(\kappa^2,\kappa)}_l \equiv \frac{1}{12\pi\sigma_0^4}\frac{1}{2l+1}\sum_m \mathrm{Real}([\kappa]_{lm}[\kappa^2]^*_{lm}) = \frac{1}{12\pi\sigma_0^4}\sum_{l_1 l_2}\mathcal{B}_{l l_1 l_2} J_{l l_1 l_2} W_l W_{l_1} W_{l_2}; \tag{14}$$

$$\begin{aligned} S^{(1)}_l &\equiv \frac{1}{16\pi\sigma_0^2\sigma_1^2} S^{(\kappa^2,\nabla^2\kappa)}_l \equiv \frac{1}{16\pi\sigma_0^2\sigma_1^2}\frac{1}{2l+1}\sum_m \mathrm{Real}([\nabla^2\kappa]_{lm}[\kappa^2]^*_{lm}) \\ &= \frac{1}{16\pi\sigma_0^2\sigma_1^2}\sum_{l_i}[l(l+1)+l_1(l_1+1)+l_2(l_2+1)]\mathcal{B}_{l l_1 l_2} J_{l l_1 l_2} W_l W_{l_1} W_{l_2}; \end{aligned} \tag{15}$$

$$\begin{aligned} S^{(2)}_l &\equiv \frac{1}{8\pi\sigma_1^4} S^{(\nabla\kappa\cdot\nabla\kappa,\nabla^2\kappa)}_l \equiv \frac{1}{8\pi\sigma_1^4}\frac{1}{2l+1}\sum_m \mathrm{Real}([\nabla\kappa\cdot\nabla\kappa]_{lm}[\nabla^2\kappa]^*_{lm}) \\ &= \frac{1}{8\pi\sigma_1^4}\sum_{l_i}\{[l(l+1)+l_1(l_1+1)-l_2(l_2+1)]l_2(l_2+1)+\text{cyclic permutation}\}\,\mathcal{B}_{l l_1 l_2} J_{l l_1 l_2} W_l W_{l_1} W_{l_2}; \end{aligned} \tag{16}$$

$$J_{l_1 l_2 l_3} \equiv \frac{I_{l_1 l_2 l_3}}{2l_3+1} = \sqrt{\frac{(2l_1+1)(2l_2+1)}{(2l_3+1)4\pi}}\begin{pmatrix} l_1 & l_2 & l_3 \\ 0 & 0 & 0 \end{pmatrix}; \tag{17}$$

$$S^{(i)} = \sum_l (2l+1) S^{(i)}_l; \tag{18}$$

$$\sigma_j^2 = \frac{1}{4\pi}\sum_l (2l+1)[l(l+1)]^j C_l W_l^2. \tag{19}$$

This set of equations constitute one of the main results of this paper. The matrices here denote the Wigner-3j symbols and W_l represents the smoothing window, for example, a top-hat, Gaussian or some form of compensated filter. Each of these spectra probes the same bispectrum $B_{l l_1 l_2}$ with different weights for individual triplets of modes that specify the bispectrum $(l, l_1 l_2)$ and define a triangle in the harmonic domain. The skew spectra is summed over all possible configurations of the bispectrum keeping one of its sides at a fixed l. For each individual choice of l, we can compute the skew spectrum $S^{(i)}_l$ relatively straightforwardly by constructing the relevant maps in real space (either by algebraic or differential operation) and then cross-correlating them in the multipole domain. Issues related to mask and noise will be dealt with in later sections, where we will show that, even in the presence of a mask, the computed skew spectra can be inverted to give an unbiased estimate of all-sky skew spectra. Presence of noise will only affect the scatter. We have explicitly displayed the experimental beam b_l in all our expressions.

To derive the above expressions, we first express the spherical harmonic expansion of the fields $[\nabla^2\kappa(\hat{\mathbf{\Omega}})]$, $[\nabla\kappa(\hat{\mathbf{\Omega}})\cdot\nabla\kappa(\hat{\mathbf{\Omega}})]$ and $[\kappa^2(\hat{\mathbf{\Omega}})]$ in terms of the harmonics of the original fields κ_{lm}. These expressions involve the 3j functions as well as factors that depend on various

l_i-dependent weight factors:

$$[\nabla^2\kappa(\hat{\boldsymbol{\Omega}})]_{lm} = \int \mathrm{d}\hat{\boldsymbol{\Omega}} Y^*_{lm}(\hat{\boldsymbol{\Omega}})[\nabla^2\kappa(\hat{\boldsymbol{\Omega}})] = -l(l+1)\kappa_{lm};$$

$$[\kappa^2(\hat{\boldsymbol{\Omega}})]_{lm} = \int \mathrm{d}\hat{\boldsymbol{\Omega}} Y^*_{lm}(\hat{\boldsymbol{\Omega}})[\kappa^2(\hat{\boldsymbol{\Omega}})] = \sum_{l_i m_i} (-1)^m \kappa_{l_1 m_1}\kappa_{l_2 m_2} I_{l_1 l_2 l} \begin{pmatrix} l_1 & l_2 & l \\ m_1 & m_2 & -m \end{pmatrix};$$

$$[\nabla\kappa(\hat{\boldsymbol{\Omega}})\cdot\nabla\kappa(\hat{\boldsymbol{\Omega}})]_{lm} = \int \mathrm{d}\hat{\boldsymbol{\Omega}} Y^*_{lm}(\hat{\boldsymbol{\Omega}})[\nabla\kappa(\hat{\boldsymbol{\Omega}})\cdot\nabla\kappa(\hat{\boldsymbol{\Omega}})] = \sum_{l_i m_i} \kappa_{l_1 m_1}\kappa_{l_2 m_2} \int \mathrm{d}\hat{\boldsymbol{\Omega}} Y^*_{lm}(\hat{\boldsymbol{\Omega}})[\nabla Y_{l_1 m_2}(\hat{\boldsymbol{\Omega}})\cdot\nabla Y_{l_2 m_2}(\hat{\boldsymbol{\Omega}})] \tag{20}$$

$$= \frac{1}{3}\sum_{l_i m_i}[l_1(l_1+1)+l_2(l_2+1)-l(l+1)] \int \mathrm{d}\hat{\boldsymbol{\Omega}} Y^*_{lm}(\hat{\boldsymbol{\Omega}}) Y_{l_1 m_1}(\hat{\boldsymbol{\Omega}}) Y_{l_2 m_2}(\hat{\boldsymbol{\Omega}})$$

$$= \frac{1}{3}\sum_{l_i m_i}(-1)^m[l_1(l_1+1)+l_2(l_2+1)-l(l+1)]\kappa_{l_1 m_1}\kappa_{l_2 m_2} I_{l_1 l_2 l} \begin{pmatrix} l_1 & l_2 & l \\ m_1 & m_2 & -m \end{pmatrix}. \tag{21}$$

We can define the power spectrum associated with the MFs through the following third-order expression:

$$V_k^{(3)} = \sum_l [V_k]_l (2l+1) = \frac{1}{6}\sum_l (2l+1)\left[S_l^{(0)} H_k(\nu) + \frac{k}{3} S_l^{(1)} H_{k-1}(\nu) + \frac{k(k-1)}{6} S_l^{(2)} H_{k-2}(\nu) + \cdots\right]. \tag{22}$$

The three skewnesses thus define triplets of MFs. At the level of two-point statistics, in the harmonic domain, we have three power spectra associated with the MF $V_k^{(3)}$ that depend on the three skew spectra we have defined. We will show later in this paper that the fourth-order correction terms too have a similar form with an additional monopole contribution that can be computed from the lower order one-point terms in a similar way to the three skewnesses defined here. The result presented here is important and implies that we can study the contributions to each of the MFs $v_k(\nu)$ as a function of the harmonic mode l. This is especially a significant result as various forms of non-Gaussianity will have different l dependence and so can potentially be distinguished from each other using this approach. The ordinary MFs add contributions from all individual l modes and hence have less power in differentiating various contributing sources of non-Gaussianity. This is one of the main motivations to extend the concept of MFs (single numbers) to 1D objects similar to power spectrum.

It is worth pointing out that the skewness and generalized skewness parameters are relatively insensitive to the background cosmology but quite sensitive to the underlying model of non-Gaussianity. The main dependence on cosmology typically results from the normalization coefficients such as σ_0 and σ_1 which are determined from the power spectrum of the convergence κ.

In real space, the skew spectra can be defined through the following correlation functions:

$$S^{(0)}(\hat{\boldsymbol{\Omega}}_1,\hat{\boldsymbol{\Omega}}_2) \equiv \langle\kappa^2(\hat{\boldsymbol{\Omega}}_1))\kappa(\hat{\boldsymbol{\Omega}}_2)\rangle; \quad S^{(1)}(\hat{\boldsymbol{\Omega}}_1,\hat{\boldsymbol{\Omega}}_2) \equiv \langle\kappa^2(\hat{\boldsymbol{\Omega}}_1)\nabla^2\kappa(\hat{\boldsymbol{\Omega}}_2)\rangle; \quad S^{(2)}(\hat{\boldsymbol{\Omega}}_1,\hat{\boldsymbol{\Omega}}_2) \equiv \langle\nabla\kappa(\hat{\boldsymbol{\Omega}}_1)\cdot\nabla\kappa(\hat{\boldsymbol{\Omega}}_1)\nabla^2\kappa(\hat{\boldsymbol{\Omega}}_2)\rangle. \tag{23}$$

Although we have adopted a harmonic approach, these correlations can equivalently be used to probe MFs especially for smaller surveys.

5 MODELLING THE PRIMORDIAL AND GRAVITY-INDUCED BISPECTRUM

It is clear that we need accurate analytical modelling of dark matter clustering for the prediction of weak-lensing statistics, but in general there is no definitive analytical theory for handling gravitational clustering in the highly non-linear regime. On larger scales, where the density field is only weakly non-linear, perturbative treatments are known to be valid. For a phenomenological statistical description of dark matter clustering in collapsed objects on non-linear scales, typically the halo model (Cooray & Seth 2002) is used. We will be using the halo model in our study, but an alternative to the halo model approach on small scales is to employ various *ansatze* which trace their origin to field-theoretic techniques. Here we provide a quick summary of some of the analytical prescriptions that can be used to model non-linear clustering. We will also provide a brief description of various models of primordial non-Gaussianity arising from variants of the inflationary universe scenario.

5.1 Hierarchical ansatz

The hierarchical *ansatz* has been used for many weak-lensing-related work, where the higher order correlation functions are constructed from the two-point correlation functions. Assuming a tree model for the matter correlation hierarchy (typically used in the highly non-linear regime), one can write the most general case, the N-point correlation function, $\langle\delta(\boldsymbol{r}_1)\ldots\delta(\boldsymbol{r}_n)\rangle_{\rm c} = \xi_N^{\delta}(\boldsymbol{r}_1,\ldots,\boldsymbol{r}_n)$ as a product of two-point correlation functions $\langle\delta(\boldsymbol{r}_i)\delta(\boldsymbol{r}_j)\rangle_{\rm c} = \xi_2^{\delta}(|\boldsymbol{r}_i-\boldsymbol{r}_j|)$ (Bernardeau et al. 2002). Equivalently, in the Fourier domain, the multispectra can be written as products of the matter power spectrum $P_{\rm lin}(k_1)$ (the temporal dependence is implicit here):

$$\xi_N(\boldsymbol{r}_1,\ldots,\boldsymbol{r}_n) \equiv \langle\delta(\boldsymbol{r}_1)\ldots\delta(\boldsymbol{r}_n)\rangle_{\rm c} = \sum_{\alpha, N=\text{trees}} Q_{N,\alpha} \sum_{\text{labellings}} \prod_{\text{edges}(i,j)}^{(N-1)} \xi_2(|\boldsymbol{r}_i-\boldsymbol{r}_j|). \tag{24}$$

It is very interesting to note that a similar hierarchy develops in the quasi-linear regime at tree level in the limiting case of vanishing variance, except that the hierarchical amplitudes become shape-dependent in such a case. These kernels are also used to relate the halo–halo correlation hierarchy to the underlying mass-correlation hierarchy. Nevertheless, there are indications from numerical simulations that these amplitudes become configuration-independent again as have been shown by high-resolution studies for the lowest order case $Q_3 = Q$ (Scoccimarro

et al. 1998; Bernardeau et al. 2002; also see Van Waerbeke et al. 2001 for related discussion about the use of PT results on intermediate scales). In Fourier space, however, such an ansatz means that the entire hierarchy of multispectra can be written in terms of sums of products of power spectra with different amplitudes $Q_{N,\alpha}$, etc. The power spectrum is defined through $\langle\delta(\boldsymbol{k}_1)\delta(\boldsymbol{k}_2)\rangle_{\rm c} = (2\pi)^3\delta_{\rm 3D}(\boldsymbol{k}_{12})P^{\delta}_{\rm nl}(k_1)$. Similarly, the bispectrum and trispectrum are defined through the following expressions: $\langle\delta(\boldsymbol{k}_1)\delta(\boldsymbol{k}_2)\delta(\boldsymbol{k}_3)\rangle_{\rm c} = (2\pi)^3\delta_{\rm 3D}(\boldsymbol{k}_{123})B^{\delta}(\boldsymbol{k}_1,\boldsymbol{k}_2,\boldsymbol{k}_3)$ and $\langle\delta(\boldsymbol{k}_1)\cdots\delta(\boldsymbol{k}_4)\rangle_{\rm c} = (2\pi)^3\delta_{\rm 3D}(\boldsymbol{k}_{1234})T^{\delta}(\boldsymbol{k}_1,\boldsymbol{k}_2,\boldsymbol{k}_3,\boldsymbol{k}_4)$. The subscript 'c' here represents the connected part of the spectrum and $\boldsymbol{k}_{i_1\ldots i_n} = \boldsymbol{k}_{i_1}+\cdots+\boldsymbol{k}_{i_n}$. The Dirac delta functions $\delta_{\rm 3D}$ ensure translation invariance at each vertex representing the multispectrum:

$$B^{\delta}(\boldsymbol{k}_1,\boldsymbol{k}_2,\boldsymbol{k}_3)_{\sum\boldsymbol{k}_i=0} = Q_3\left[P^{\delta}_{\rm nl}(k_1)P^{\delta}_{\rm nl}(k_2)+P^{\delta}_{\rm nl}(k_1)P^{\delta}_{\rm nl}(k_3)+P^{\delta}_{\rm nl}(k_2)P^{\delta}(k_3)\right]; \tag{25}$$

$$T^{\delta}(\boldsymbol{k}_1,\boldsymbol{k}_2,\boldsymbol{k}_3,\boldsymbol{k}_4)_{\sum\boldsymbol{k}_i=0} = R_a\Big[P^{\delta}_{\rm nl}(k_1)P^{\delta}_{\rm nl}(k_2)P^{\delta}_{\rm lin}(k_3)+\text{cyclic permutation}]+R_b[P^{\delta}_{\rm nl}(k_1)P^{\delta}_{\rm nl}(|\boldsymbol{k}_{12}|)P^{\delta}_{\rm nl}(|\boldsymbol{k}_{123}|)+\text{cyclic permutation}\Big]. \tag{26}$$

Different hierarchical models differ in the way numerical values are allocated to the different amplitudes. Bernardeau & Schaeffer (1992) considered 'snake', 'hybrid' and 'star' diagrams with differing amplitudes at various order. A new 'star' appears at each order. Higher order 'snakes' or 'hybrid' diagrams are built from lower order 'star' diagrams. In models where we have only star diagrams (Valageas et al. 2004), the expressions for the trispectrum takes the following form: $T^{\delta}(\boldsymbol{k}_1,\boldsymbol{k}_2,\boldsymbol{k}_3,\boldsymbol{k}_4)_{\sum\boldsymbol{k}_i=0} = Q_4[P^{\delta}_{\rm nl}(k_1)P^{\delta}_{\rm nl}(k_2)P^{\delta}_{\rm nl}(k_3)+\text{cyclic permutation}]$. Following Valageas et al. (2004), we will call these models 'stellar models'. Indeed, it is also possible to use perturbative calculations which are, however, valid only at large scales. While we still do not have an exact description of the non-linear clustering of a self-gravitating medium in a cosmological scenario, these approaches do capture some of the salient features of gravitational clustering in the highly non-linear regime and have been tested extensively against numerical simulations in 2D statistics of convergence of shear (Valageas et al. 2004). These models have also been used for modelling the covariance of lower order cumulants (Munshi & Valageas 2005).

The statistics of the projected convergence field can be constructed using a suitably defined variable $\eta = (\kappa-\kappa_{\rm min})/\kappa_{\rm min}$, where $\kappa(\hat{\boldsymbol{\Omega}},r_{\rm s}) = -\int_0^{r_{\rm s}}{\rm d}r\,w(r,r_{\rm s})$. The variable η follows the same statistics as the density parameter δ, and under some simplifying assumptions and using hierarchical ansatze, it can be shown that $S^{(0)} = S^{\delta}_3/\eta$, and similar results also hold at higher order, that is, $K^{(0)} = K^{\delta}_4/\eta^2$. The overall dependance on the cosmology is absorbed in the definition of η, and the skewness $S^{\delta}_3 = 3Q$ and kurtosis $K^{\delta}_4 = 4R_a+12R_b\sim 16Q_4$ parameters, defined in terms of the hierarchical amplitudes, Q_3 and R_a, R_b, respectively, are insensitive to the background cosmology (Hui 1999; Munshi 2000; Munshi & Coles 2000; Munshi & Jain 2001).

5.2 Halo model

The halo model relies on a phenomenological model for the clustering of haloes and predictions from perturbative calculations on large scales to model the non-linear correlation functions. The halo overdensity at a given position $\boldsymbol{x}$, $\delta^{\rm h}(\boldsymbol{x},M;z)$, can be related to the underlying density contrast $\delta(\boldsymbol{x},z)$ by a Taylor expansion (Mo, Jing & White 1997):

$$\delta^{\rm h}(\boldsymbol{x},M;z) = b_1(M;z)\delta(\boldsymbol{x},z)+\frac{1}{2}b_2(M,z)\delta^2(\boldsymbol{x},z)+\cdots. \tag{27}$$

The expansion coefficients are functions of the threshold $\nu_{\rm c} = \delta_{\rm c}/\sigma(M,z)$. Here $\delta_{\rm c}$ is the threshold for a spherical overdensity to collapse and $\sigma(M,z)$ is the *rms* fluctuation within a top-hat filter. The halo model incorporates perturbative aspects of gravitational dynamics by using it to model the halo–halo correlation hierarchy; the non-linear features of this take direct contributions from the halo profile. The total power spectrum $P^{\rm t}(k)$ at non-linear scale can be written as

$$P^{\rm 1h} = I^0_2(k,k);\qquad P^{\rm 2h}(k) = \left[I^1_1(k)\right]^2P^{\delta}_{\rm lin}(k);\qquad P^{\rm t} = P^{\rm 2h}(k)+P^{\rm 1h}(k) \tag{28}$$

(Seljak 2000). The minimum halo mass that we consider in our calculation is $10^3\,{\rm M}_{\odot}$ and the maximum is $10^{16}\,{\rm M}_{\odot}$. More massive haloes do not contribute significantly owing to their low abundance. The bispectrum involves terms from one-, two- or three-halo contributions and the total can be written as

$$B^{\rm t}(k_1,k_2,k_3) = B^{\rm 3h}(k_1,k_2,k_3)+B^{\rm 2h}(k_1,k_2,k_3)+B^{\rm 1h}(k_1,k_2,k_3); \tag{29}$$

$$B^{\rm 1h} = I^0_3(k_1,k_2,k_3);\quad B^{\rm 2h}(k_1,k_2,k_3) = I^1_2(k_1,k_2)I^0_1(k_3)P^{\delta}_{\rm lin}(k_3)+\text{cyclic permutation}; \tag{30}$$

$$B^{\rm 3h}(k_1,k_2,k_3) = \left[2J(k_1,k_2,k_3)I^1_1(k_3)+I^2_1(k_3)\right]I^1_1(k_1)I^1_1(k_2)P^{\delta}_{\rm lin}(k_1)P^{\delta}_{\rm lin}(k_2)+\text{cyclic permutation}. \tag{31}$$

The kernel $J(k_1,k_2,k_3)$ is derived using second-order PT (Fry 1984; Bouchet et al. 1992), and the integrals I^{β}_{μ} can be expressed in terms of the Fourier transform of halo profile, assumed to be an NFW profile (Navarro, Frenk & White 1996), as

$$I^{\beta}_{\mu}(k_1,k_2,\ldots,k_{\mu};z) = \int{\rm d}M\left(\frac{M}{\rho_{\rm b}}\right)^{\mu}\frac{{\rm d}n(m,z)}{{\rm d}M}b_{\beta}(M)y(k_1,M)\ldots y(k_{\mu},M);\quad y(k,M) = \frac{1}{M}\int_0^{r_v}{\rm d}r4\pi r^2\rho(r,M)\left[\frac{\sin(kr)}{kr}\right]. \tag{32}$$

The mass function is assumed to be given by the Press–Schechter form (Press & Schechter 1974). The results are obtained by substituting equations (29)–(31) into equations (12) and (13). The convergence power spectra and bispectra thus computed are then substituted into equation (19).

Results from the halo model analysis are plotted for the skew spectra $S^{(0)}_l$ (left-hand panel), $S^{(1)}_l$ (middle panel) and $S^{(2)}_l$ (right-hand panel). The source redshift is fixed at unity. The underlying background cosmology is that of the *WMAP*7. No smoothing window was assumed. A

sharp cut-off at $l_{\rm max} = 2000$ was used for this calculation. As mentioned, haloes in the mass range 10^3–$10^{16}\,{\rm M}_\odot$ were used in this calculation. The halo model expression for the bispectrum is defined in equations (29)–(31).

5.3 Perturbative calculations in the quasi-linear regime and their extensions

In the weakly non-linear regime ($\delta \leq 1$), the description of gravitational clustering can be described by PT (Bernardeau et al. 2002). However, the perturbative treatment breaks down when density contrast at a given length-scale becomes non-linear ($\delta \geq 1$) which significantly increases the growth of clustering. Perturbative studies of gravitational clustering have attracted a lot of attention. Starting with Peebles (1980), there have been many attempts to reproduce the clustering of a self-gravitating fluid in a cosmological setting; it is typically tackled by brute force using N-body simulations (Bernardeau et al. 2002). Expanding the density contrast in a Fourier series, and assuming the density contrast is less than unity, for the pertubative series to be convergent, we get

$$\delta(\boldsymbol{k}) = \delta^{(1)}(\boldsymbol{k}) + \delta^{(2)}(\boldsymbol{k}) + \delta^{(3)}(\boldsymbol{k}) + \cdots; \quad \delta^{(2)}(k) = \int \frac{{\rm d}^3k_1}{2\pi} \int \frac{{\rm d}^3k_2}{2\pi} \delta_{\rm D}(\boldsymbol{k}_1 + \boldsymbol{k}_2 - \boldsymbol{k}) F_2(k_1, k_2) \delta^{(1)}(\boldsymbol{k}_1) \delta^{(1)}(\boldsymbol{k}_2). \tag{33}$$

The linearized solution for the density field is $\delta^{(1)}(\boldsymbol{k})$; higher order terms yield corrections to this linear solution. Using a fluid approach known to be valid at large scales (and before shell crossing), one can write the second-order correction to the linearized density field using the kernel $F_2(\boldsymbol{k}_1, \boldsymbol{k}_2)$. Newtonian gravity coupled to the Euler and continuity equations employed to solve a system of non-linear coupled integro-differential equations reproduces the kernels $F_2(k_1, k_2)\, F_3(k_1, k_2, k_3)$ when solved perturbatively order by order. The matter bispectrum can be expressed in terms of an effective fitting formula that can interpolate between the quasi-linear regime and the highly non-linear regime (Takada & Jain 2003):

$$B^{\delta}_{\rm nl}(\boldsymbol{k}_1, \boldsymbol{k}_2, \boldsymbol{k}_3) = 2F_2(\boldsymbol{k}_1, \boldsymbol{k}_2) P^{\delta}_{\rm lin}(\boldsymbol{k}_1) P^{\delta}_{\rm lin}(\boldsymbol{k}_2) + \text{cyclic permutation};$$

$$F_2(\boldsymbol{k}_1, \boldsymbol{k}_2) = \frac{5}{7} a(n_{\rm e}, k) a(n_{\rm e}, k) + \left(\frac{\boldsymbol{k}_1 \cdot \boldsymbol{k}_2}{2k_2^2} + \frac{\boldsymbol{k}_1 \cdot \boldsymbol{k}_2}{2k_1^2} \right) b(n_{\rm e}, k) b(n_{\rm e}, k) + \frac{2}{7} \left(\frac{\boldsymbol{k}_1 \cdot \boldsymbol{k}_2}{k_1 k_2} \right)^2 c(n_{\rm e}, k) c(n_{\rm e}, k). \tag{34}$$

The coefficients $a(n_{\rm e}, k)$, $b(n_{\rm e}, k)$ and $c(n_{\rm e}, k)$ are defined as follows (Takada & Jain 2003):

$$a(n_{\rm e}, k) = \frac{1 + \sigma_8^{-0.2}(z) \sqrt{(q/4)^{n_{\rm e}+3.5}}}{1 + (q/4)^{n_{\rm e}+3.5}}; \quad b(n_{\rm e}, k) = \frac{1 + 0.4(n_{\rm e} + 3) q^{n_{\rm e}+3}}{1 + q^{n_{\rm e}+3}}; \quad c(n_{\rm e}, k) = \frac{(2q)^{n_{\rm e}+3}}{1 + (2q)^{n_{\rm e}+3.5}} \left\{ 1 + \left[\frac{4.5}{1.5 + (n_{\rm e} + 3)^4} \right] \right\}. \tag{35}$$

Here $n_{\rm e}$ is the effective spectral slope associated with the linear power spectra, $n_{\rm e} = {\rm d} \ln P_{\rm lin} / {\rm d} \ln k$, q is the ratio of a given length-scale to the non-linear length-scale, $q = k/k_{\rm nl}$, where $k^3/2\pi^2 D^2(z) P_{\rm lin}(k_{\rm nl}) = 1$ and $Q_3(n_{\rm e}) = (4 - 2^{n_{\rm e}})/(1 + 2^{n_{\rm e}})$. Similarly, $\sigma_8(z) = D(z)\sigma_8$. At length-scales where $q \ll 1$, which means the relevant length-scales are well within the quasi-linear regime, $a = b = c = 1$ and we recover the tree-level perturbative results. In the regime where $q \gg 1$ and the length-scales we are considering are well within the non-linear scale, we recover $a = \sigma_r^{-0.2}(z) \sqrt{0.7 Q_3(n_{\rm e})}$ with $b = c = 0$. In this limit, the bispectrum becomes independent of configuration and we recover the hierarchical form of bispectrum discussed before. However, whether there are weak violations of hierarchical ansatz in the highly non-linear regime is still not clear and can only be determined through higher resolution N-body simulations when they are available. Similar fitting functions for dark energy dominated universe calibrated against simulations are also available, and at least in the quasi-linear regime, most of the difference comes from the linear growth factor (Ma et al. 1999). The analytical modelling of the matter bispectrum presented here is equivalent to the so-called halo model predictions presented above.

We have used this model to construct the analytical predictions for various skewness parameters and the corresponding skew spectra. The results are plotted in Figs 3–7. In Fig. 3, we have plotted the three skewness parameters $S^{(0)}$, $S^{(1)}$ and $S^{(2)}$ as a function of the smoothing angular scales $\theta_{\rm s}$ as defined in equation (9) for sources at a fixed redshift $z_{\rm s} = 1$. In Fig. 4, we change the source redshift to compare predictions. Two different source redshifts are considered, $z_{\rm s} = 0.5$ and 1.0. In total, we compare three different redshifts, $z_{\rm s} = 0.5$, 1.0 and 1.5. We use

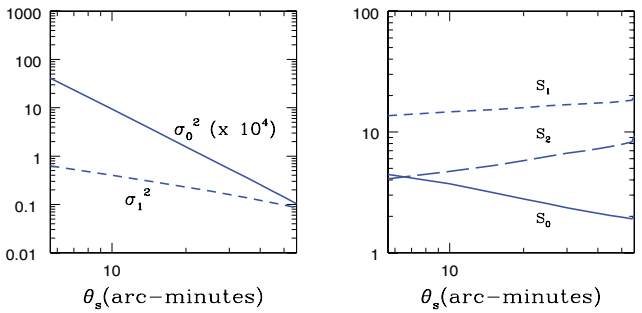

Figure 3. The moments $\sigma_0^2(\theta_{\rm s})$ and $\sigma_1^2(\theta_{\rm s})$ (left-hand panel) and the skewness paramters $S^{(0)}(\theta_{\rm s})$, $S^{(1)}(\theta_{\rm s})$ and $S^{(2)}(\theta_{\rm s})$ (right-hand panel) are plotted for the source redshift $z_{\rm s} = 1$ as a function of the smoothing angular scale $\theta_{\rm s}$ [see equation (19) for the definitions of σ_i and $S^{(n)}$]. The underlying cosmology is assumed to be that of the *WMAP*7. A top-hat window is assumed for both these plots. The resolution is fixed at $l_{\rm max} = 4000$. The underlying modelling of the convergence bispectrum $\mathcal{B}_{l_1 l_2 l_3}$ depends on the modelling of the matter bispectrum $B_{l_1 l_2 l_3}$. The specific model for the underlying model that was used for this plot is based on perturbative results and its extrapolation to a highly non-linear regime (see text for more details). The skewness paramaters are defined in equation (9). The parameters σ_j are defined in equation (19).

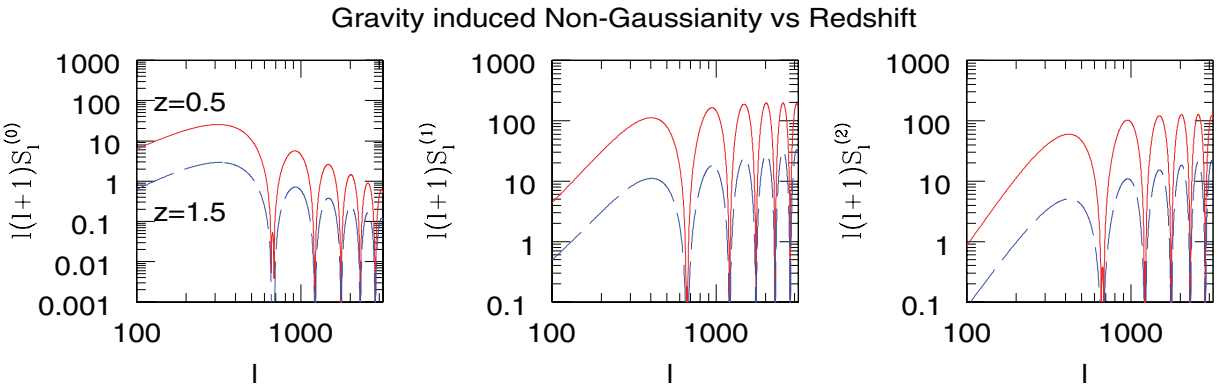

Figure 7. The skew spectra $S_l^{(0)}$, $S_l^{(1)}$ and $S_l^{(2)}$ are plotted for $z_s = 0.5$ (solid line) and 1.5 (dashed line) as a function of the wavenumber l. The underlying cosmology is that of the *WMAP*7. A top-hat window is assumed. Various curves correspond to different smoothing angular scales as indicated. The resolution is fixed at $l_{max} = 4000$. The smoothing angular scale is fixed at $\theta_s = 25$ arcmin. Note that the use of a broader window not only removes power at smaller angular scales, but also changes the overall normalization of the skew spectra. The skew spectra for any specific smoothing angular scales increase with lowering of the source redshift. This is due to the fact that the probability distribution function of convergence for higher redshift is more Gaussian than at a lower redshift. At a lower redshift, the highly evolved LSS results in higher departure of the convergence statistics from Gaussianity.

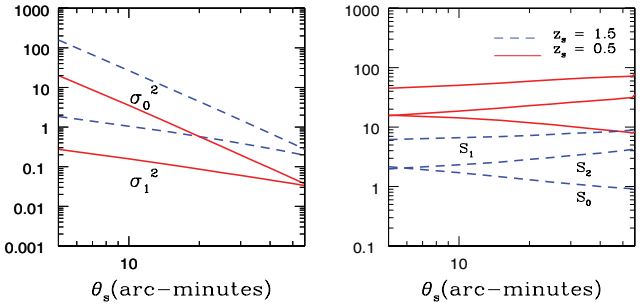

Figure 4. Same as the previous figure but for the redshifts $z_s = 0.5$ and 1.5 as indicated. The skewness paramaters are defined in equation (9). The parameters σ_j^2 are defined in equation (19). For a given angular smoothing, the skewness parameters increase with redshift. The cosmological parameters of the background cosmology is that of the *WMAP*7. The variance parameters σ_j^2 increase with redshift; however, the skewness parameters show an increasing trend.

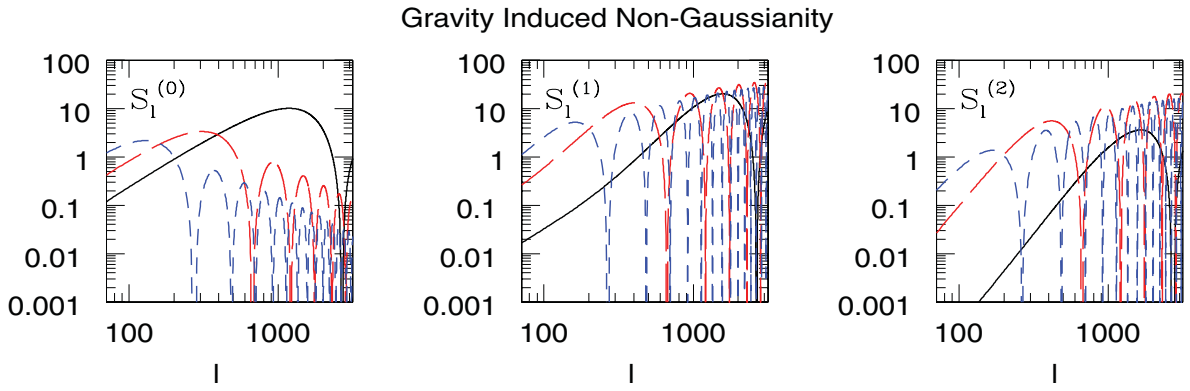

Figure 6. The skew spectra $S_l^{(0)}$, $S_l^{(1)}$ and $S_l^{(2)}$ are plotted for $z_s = 1$ as a function of the wavenumber l. The underlying cosmology is that of the *WMAP*7. A top-hat window is assumed. Various curves correspond to different smoothing angular scales as indicated. The resolution is fixed at $l_{max} = 4000$. The smoothing angular scales considered are $\theta_s = 5$ arcmin (solid lines), 25 arcmin (long-dashed lines) and 55 arcmin (short-dashed lines), respectively. The skew pectra are defined in equation (19). The underlying bispectrum is constructed using the analytical model prescribed in equation (34). It is interesting to note that at smaller l the skew spectra with larger smoothing angular scales dominate. However, smaller smoothing angular scales dominate at higher l, resulting in higher values of the corresponding one-point skewness parameters.

top-hat filters with different angular smoothing scales. The skew spectra, defined in equation (19), are integrated measures and their value at a specific harmonic depends on the modelling of the bispectrum for the entire range of harmonics being considered. The skew spectra are plotted as functions of harmonic l in Figs 6 and 7. In Fig. 6, we have fixed the redshift $z_s = 1.0$ and changed the smoothing angular scale θ_s. We consider three smoothing scales, $\theta_s = 5$, 25 and 55 arcmin. In Fig. 7, results for two different redshifts, $z_s = 0.5$ and 1.5, are compared

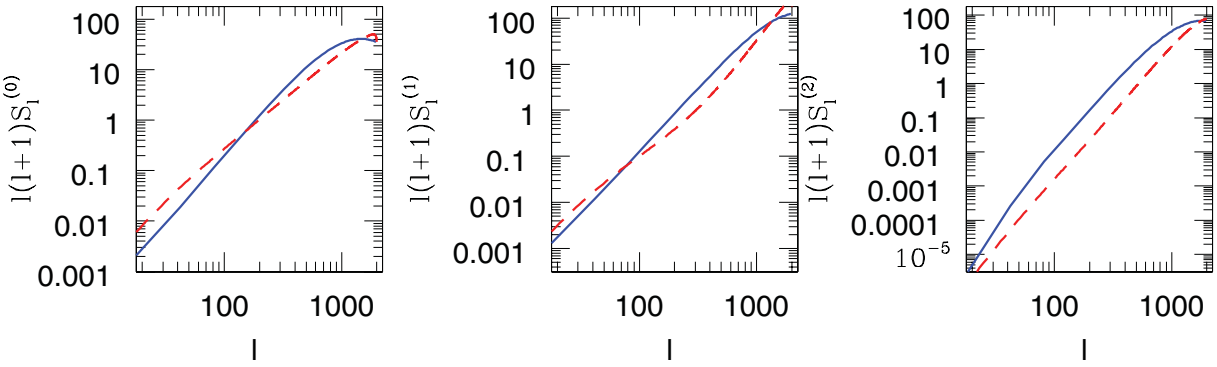

Figure 5. The halo model is used to predict the skew spectra $S_l^{(0)}$ (left-hand panel), $S_l^{(1)}$ (middle panel) and $S_l^{(2)}$ (right-hand panel). The source redshift is fixed at unity. The underlying background cosmology is that of the *WMAP*7. No smoothing window was assumed. A sharp cut-off at $l_{\rm max} = 2000$ was used for these calculations. Haloes in the mass range of 10^3–$10^{16}\,{\rm M}_\odot$ were included in these calculations. The halo model expression for the bispectrum is defined in equations (29)–(31). The dashed lines correspond to the analytical model prescribed in equation (34).

for a fixed angular smoothing scale $\theta_{\rm s} = 25$ arcmin. The oscillatory behaviour seen in these plots is due to our choice of filter function, that is, top-hat window.

We have compared and plotted the PT results and the halo model predictions for the three skew spectra in Fig. 5 as a function of the angular harmonics l for a source redshift $z_{\rm s} = 1$. The results show broad agreement between the two models for the choice of our background cosmology and the source redshift distribution.

5.4 Primordial non-Gaussianity: bispectrum

A recent (controversial) claim of a detection of non-Gaussianity (Yadav & Wandelt 2008) in the *WMAP*5 sky maps has boosted interest in cosmological non-Gaussianity. Much of the interest in primordial non-Gaussianity has focused on a phenomenological '*local* $f_{\rm NL}$' parametrization in terms of the perturbative non-linear coupling in the primordial curvature perturbation (Verde et al. 2000):

$$\Phi(x) = \Phi_{\rm L}(x) + f_{\rm NL}\left(\Phi_{\rm L}^2(x) - \left\langle \Phi_{\rm L}^2(x)\right\rangle\right), \tag{36}$$

where $\Phi_{\rm L}(x)$ denotes the linear Gaussian part of the Bardeen curvature and $f_{\rm NL}$ is the non-linear coupling parameter. A number of models have non-Gaussianity which can be approximated by this form. The leading-order non-Gaussianity present in this model is at the level of the bispectrum, or in configuration space at the three-point level. Many studies involving primordial non-Gaussianity have used the bispectrum, motivated by the fact that it contains all the information about $f_{\rm NL}$ (Babich 2005). This model has been extensively studied (Creminelli 2003; Komatsu, Spergel & Wandelt 2005; Cabella et al. 2006; Creminelli et al. 2006; Medeiros & Contaldi 2006; Smith, Senatore & Zaldarriaga 2009), with most of the measurements providing convolved estimates of the bispectrum. It is interesting to note here, in the context of bispectrum estimation from CMB sky, optimized three-point estimators were introduced by Heavens (1998) and have been successively developed (Smith et al. 2000; Komatsu et al. 2005; Creminelli et al. 2006; Smith & Zaldarriaga 2006; Creminelli, Senatore & Zaldarriaga 2007b) to the point where an estimator for $f_{\rm NL}$ which saturates the Cramer–Rao bound exists for partial sky coverage and inhomogeneous noise (Smith et al. 2009). Approximate forms also exist for *equilateral* non-Gaussianity, which may arise in models with non-minimal Lagrangian with higher derivative terms (Chen et al. 2007a; Chen, Easther & Lim 2007b). In these models, the largest signal comes from spherical harmonic modes with $\ell_1 \simeq \ell_2 \simeq \ell_3$, whereas for the local model, the signal is highest when one ℓ is much smaller than the other two – the so-called *squeezed* configuration.

In the Fourier space, the primordial bispectrum of local type defined in equation (36) takes the following form:

$$B_\delta^{\rm loc}(\boldsymbol{k}_1\boldsymbol{k}_1, \boldsymbol{k}_3) = 2 f_{\rm NL}^{\rm loc}\left[P_{\rm lin}^\Phi(k_1)P_{\rm lin}^\Phi(k_2) + \text{cyclic permutation}\right]. \tag{37}$$

The primordial potential power spectrum in standard inflationary models takes a power-law form $P^\Phi(k) \propto k^{n-4}$. In the linear regime, the primordial bispectrum for the density field $B_\delta^{\rm prim}$ in case of a local model evolves according to the following expression (see Hikage et al. 2006 for a detailed derivation and discussion):

$$B_\delta^{\rm loc}(\boldsymbol{k}_1\boldsymbol{k}_1, \boldsymbol{k}_3; z) = \frac{2 f_{\rm NL}^{\rm loc}}{D(z)}\left[\frac{\mathcal{M}(k_3)}{\mathcal{M}(k_1)\mathcal{M}(k_2)}P_{\rm lin}^\delta(k_1, z)P_{\rm lin}^\delta(k_2, z) + \text{cyclic permutation}\right]; \tag{38}$$

$$\delta(\boldsymbol{k}, z) = D(z)\mathcal{M}(k)\Phi(\boldsymbol{k}, z); \quad \mathcal{M}(k) \equiv -\frac{2}{3H_0^2\Omega_{\rm M}}k^2T(k). \tag{39}$$

Here $D(z)$ is the linear growth factor normalized such that $D(z) \to 1/(1+z)$ and $T(k)$ is the transfer function given by an approximate expression found in Bardeen et al. (1986). According to standard inflationary predictions, $P^\Phi(k) \propto k^{n-4}$, and the linear power spectra for the density is given by $P_{\rm lin}^\delta(k, z) = D^2(z)\mathcal{M}(k)^2P^\Phi(k)$. The primordial bispectrum for the density can similarly be expressed in terms of that of the primordial potential perturbations $B_\delta^{\rm prim}(k_1, k_2, k_3, z) = D^3(z)\mathcal{M}(k_1)\mathcal{M}(k_2)\mathcal{M}(k_3)B_\Phi^{\rm prim}(k_1, k_2, k_3)$. The primordial potential bispectrum

for the equilateral type can be expressed as (Creminelli et al. 2006)

$$B_{\phi}^{\rm equi} = 6 f_{\rm NL}^{\rm equi} \left\{ -[P_\Phi(k_1)P_\Phi(k_2) + \text{cyclic permutation}] - 2[P_\Phi(k_1)P_\Phi(k_2)P_\Phi(k_3)]^{2/3} + \left[P_\Phi^{1/3}(k_1)P_\Phi^{2/3}(k_2)P_\Phi(k_2) + \text{cyclic permutation} \right] \right\}. \tag{40}$$

The primordial density bispectrum for the equilateral case $B_\delta^{\rm equi}$ can be expressed, following the same procedure as followed for the local type, as

$$\begin{aligned} B_\delta^{\rm equi}(\boldsymbol{k}_1, \boldsymbol{k}_1, \boldsymbol{k}_3; z) = \frac{6 f_{\rm NL}^{\rm equi}}{D(z)} \Bigg[& - \left[\frac{\mathcal{M}(k_3)}{\mathcal{M}(k_1)\mathcal{M}(k_2)} P_{\rm lin}^\delta(k_1, z) P_{\rm lin}^\delta(k_2, z) + \text{cyclic permutation} \right] \\ & -2 \left[\mathcal{M}(k_1)\mathcal{M}(k_2)\mathcal{M}(k_3) \right]^{-1/3} \left[P_{\rm lin}^\delta(k_1, z) P_{\rm lin}^\delta(k_2, z) P_{\rm lin}^\delta(k_3, z) \right]^{2/3} \\ & + \left\{ \frac{\mathcal{M}(k_1)^{1/3}}{\mathcal{M}(k_2)^{1/3}\mathcal{M}(k_3)} \left[P_{\rm lin}^\delta(k_1, z) P_{\rm lin}^\delta(k_2, z)^2 P_{\rm lin}^\delta(k_3, z)^3 \right]^{1/3} + \text{cyclic permutation} \right\} \Bigg]. \end{aligned} \tag{41}$$

However, in contrast to the local model, in the equilateral model, the functional forms of the expressions do not have any connection to fundamental physics but are just fits where the exact expressions are more complicated. The folded or flattened model that is maximized for $k_2 \approx k_3 \approx k_1/2$ is well approximated by the following form:

$$B_\phi^{\rm fold} = 6 f_{\rm NL}^{\rm fold} \left\{ [P_\Phi(k_1)P_\Phi(k_2) + \text{cyclic permutation}] + 3[P_\Phi(k_1)P_\Phi(k_2)P_\Phi(k_3)]^{2/3} - \left[P_\Phi^{1/3}(k_1)P_\Phi^{2/3}(k_2)P_\Phi(k_2) + \text{cyclic permutation} \right] \right\}. \tag{42}$$

In terms of the density perturbations, we get the following expression:

$$\begin{aligned} B_\delta^{\rm fol}(\boldsymbol{k}_1, \boldsymbol{k}_1, \boldsymbol{k}_3; z) = \frac{6 f_{\rm NL}^{\rm fol}}{D(z)} \Bigg[& \left[\frac{\mathcal{M}(k_3)}{\mathcal{M}(k_1)\mathcal{M}(k_2)} P_{\rm lin}^\delta(k_1, z) P_{\rm lin}^\delta(k_2, z) + \text{cyclic permutation} \right] \\ & 3 \left[\mathcal{M}(k_1)\mathcal{M}(k_2)\mathcal{M}(k_3) \right]^{-1/3} \left[P_{\rm lin}^\delta(k_1, z) P_{\rm lin}^\delta(k_2, z) P_{\rm lin}^\delta(k_3, z) \right]^{2/3} \\ & - \left\{ \frac{\mathcal{M}(k_1)^{1/3}}{\mathcal{M}(k_2)^{1/3}\mathcal{M}(k_3)} \left[P_{\rm lin}^\delta(k_1, z) P_{\rm lin}^\delta(k_2, z)^2 P_{\rm lin}^\delta(k_3, z)^3 \right]^{1/3} + \text{cyclic permutation} \right\} \Bigg]. \end{aligned} \tag{43}$$

The folded or flattened form of bispectrum appears in canonical single-field models where the initial Bunch–Davies vacuum is modified.

The evolution of the primordial bispectrum is different from that generated by gravitational evolution. The angular dependence for the gravitationally induced bispectrum is also different. On large angular scales, which will be probed by future weak-lensing surveys, gravitational instability may not have erased the memory of primordial non-Gaussianity, which can provide supplementary information to results obtained from CMB observations.

In Fig. 8, we display the results for skew spectra from local-type primordial non-Gaussianity. Three different smoothing angular scales are considered, $\theta_{\rm s} = 5$, 25 and 55 arcmin, respectively. All sources have redshift fixed at unity, that is, $z_{\rm s} = 1$. The oscillations seen in various plots are characteristics of the top-hat window we have used. The normalization of the primordial bispectrum is fixed at unity, that is, $f_{\rm NL}^{\rm loc} = 1$. In Fig. 9, we plot the skew spectra for three different types of primordial non-Gaussianity: local, equilateral and folded. We consider a top-hat smoothing with radius $\theta_{\rm s} = 25$ arcmin and all sources have redshift fixed at unity, that is, $z_{\rm s} = 1$. The normalization of all primordial bispectrum types is held fixed at unity, that is, $f_{\rm NL}^{\rm loc} = f_{\rm NL}^{\rm equi} = f_{\rm NL}^{\rm fold} = 1$. In Fig. 10, skew spectra for local-type primordial non-Gaussianity are studied as functions of source redshift and compared against gravity-induced non-Gaussianity. Two different source redshifts are considered,

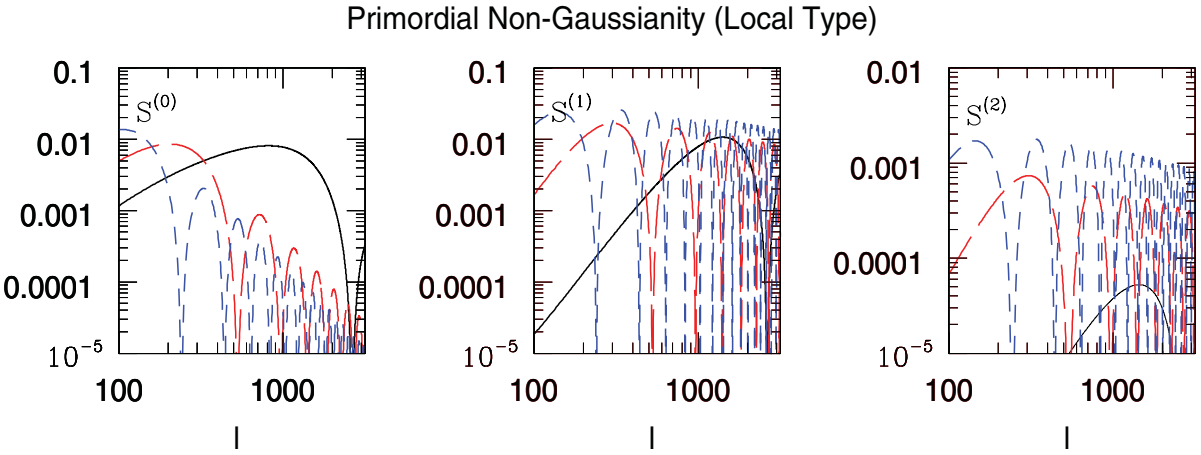

Figure 8. The skew spectra $S_l^{(0)}$, $S_l^{(1)}$ and $S_l^{(2)}$ are plotted for source redshift $z_{\rm s} = 1.0$ as a function of the wavenumber l. The skew spectra correspond to the primordial bispectrum of local type (equation 39). The normalization coefficient is set to unity, $f_{\rm NL}^{\rm loc} = 1$. The underlying cosmology is that of the *WMAP*7. A top-hat window is assumed. Various curves correspond to different smoothing angular scales as indicated. The resolution is fixed at $l_{\rm max} = 2000$. The three angular scales that we plot correspond to $\theta_{\rm s} = 5$ arcmin (solid lines), 25 arcmin (long-dashed lines) and 55 arcmin (short-dashed lines), respectively.

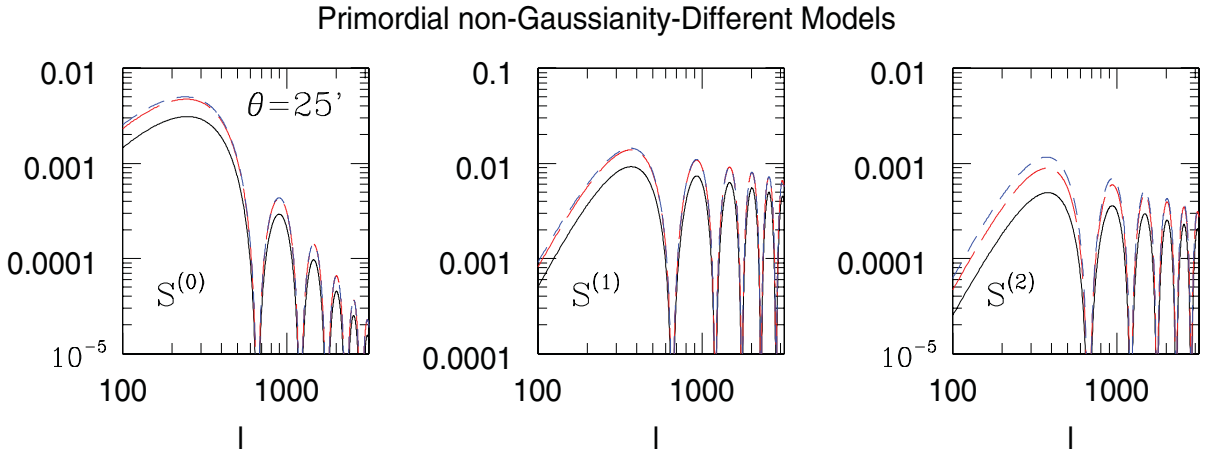

Figure 9. The skew spectra $S_l^{(0)}$, $S_l^{(1)}$ and $S_l^{(2)}$ are plotted. The smoothing angular scale is $\theta_s = 25$ arcmin. The three different models that are depicted are local (solid lines), equilateral (long-dashed lines) and folded (short-dashed lines) models. These models are defined by equations (39), (41) and (43), respectively. The redshift is fixed at unity, $z_s = 1$. All the non-Gaussianity parameters describing various models are fixed at unity, that is, $f_{\rm NL}^{\rm loc} = 1$, $f_{\rm NL}^{\rm equi} = 1$ and $f_{\rm NL}^{\rm fold} = 1$.

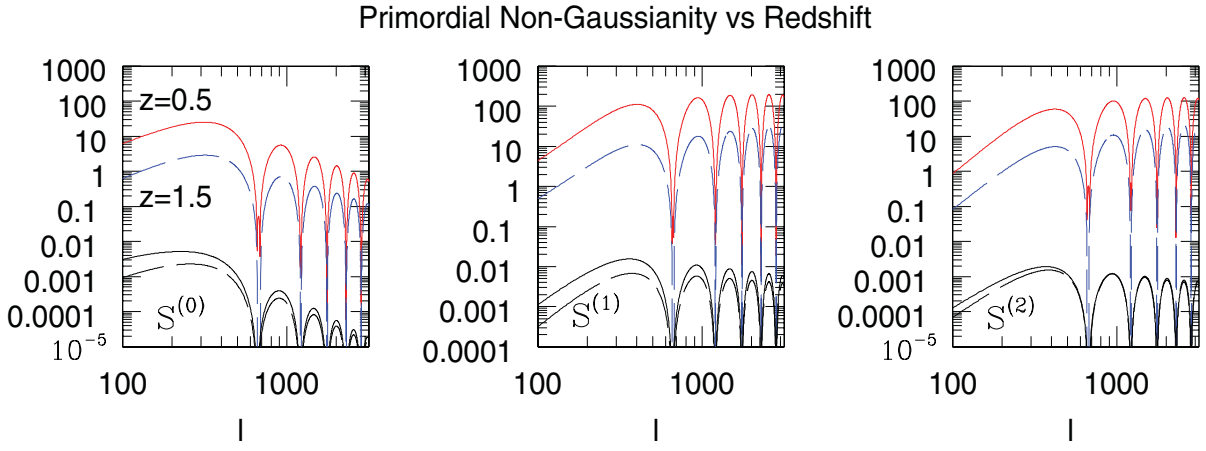

Figure 10. The skew spectra $S_l^{(0)}$, $S_l^{(1)}$ and $S_l^{(2)}$ are plotted for two different source redshifts, $z_s = 1.5$ (long-dashed lines) and $z_s = 0.5$ (solid lines) as a function of the wavenumber l. The lower pair of curves in each panel correspond to primordial bispectra of local type. The gravity-induced skew spectra that dominate all scales at each redshift are also shown for comparison (upper pairs of curves).

$z_s = 0.5$ and 1.5. It is clear from these plots that gravity-induced non-Gaussianity is dominant contribution at all angular scales and for all redshifts. The shapes of the skew spectra for various sources are very similar and reflect the choice of projection kernel.

6 ESTIMATORS AND THEIR SCATTER

As noted above, the estimators for the skew spectra can be most easily computed by cross-correlating maps in the harmonic domain. These maps are constructed in real space by applying various derivative operators. The recovered skew spectra will depend on the mask, if one is present, because a mask typically introduces mode–mode coupling. The approach we adopt here to reconstruct the unbiased power spectra in such a case is the pseudo-$\mathcal{C}_l$ method (Hivon et al. 2002). This approach depends on expressing the observed power spectra $\mathcal{C}_l$ in the presence of a mask as a linear combination of unbiased all-sky power spectra.

The three different generalized skew spectra that we have introduced here can be thought of as cross-spectra of relevant fields. We denote these generic fields by A and B and will denote the generic skew spectra by $S_l^{[A,B]}$. The skew spectra recovered in the presence of a mask is given by $\tilde{S}_l^{[A,B]}$ and the unbiased estimator is denoted by $\hat{S}_l^{[A,B]}$. The skew spectra recovered in the presence of a mask, $\tilde{S}_l^{[A,B]}$, will be biased. However, to construct an unbiased estimator $\hat{S}_l^{[A,B]}$ for the skew spectra, the following procedure is sufficient. The derivation follows the same arguments as detailed in Munshi, Smidt & Cooray (2010) and will not be reproduced here. The skew spectra measured from the data, also known as the pseudo-skew spectra, $\tilde{S}_l^{[A,B]}$, are a linear combination of the underlying unbiased skew spectra $\hat{S}_l^{[A,B]}$. The exact nature of the linear combinations is encoded in the matrix $M_{ll'}$ which depends on observational details such as the mask and the binning of the angular

harmonics l:

$$\tilde{S}_l^{[A,B]} = \frac{1}{2l+1}\sum_m \tilde{A}_{lm}\tilde{B}^*_{lm}; \quad \tilde{S}_l^{[A,B]} = \sum_{l'} M_{ll'} S_l^{[A,B]}; \quad M_{ll'} = \frac{1}{2l+1}\sum_{l'l''} I^2_{ll'l''}|w_{l''}|^2; \quad \{A,B\} \in \left\{\kappa, \kappa^2, (\nabla\kappa\cdot\nabla\kappa), \nabla^2\kappa\right\}. \tag{44}$$

The mode–mode coupling matrix M is constructed from the power spectra of the mask $w_{l''}$ and used for estimation of unbiased skew spectra $\hat{S}_{l'}^{[A,B]}$. Typically, the mask consists of bright stars and saturated spikes where no lensing measurements can be performed. The results that we present here are generic. The estimator thus constructed is an unbiased estimator. The computation of the scatter covariance of the estimates can be done using analytical methods, thereby avoiding the need of expensive Monte Carlo (MC) simulations. The scatter or covariance of the unbiased estimates $\langle\delta\hat{S}_l^{[A,B]}\delta\hat{S}_{l'}^{[A,B]}\rangle$ is related to that of the direct estimates $\langle\delta\tilde{S}_l^{[A,B]}\delta\tilde{S}_{l'}^{[A,B]}\rangle$ from the masked sky by a similarity transformation. The transformation is given by the same mode-coupling matrix M:

$$\hat{S}_l^{[A,B]} = \sum_{l'}[M^{-1}]_{ll'}\tilde{S}_{l'}^{[A,B]}; \quad \left\langle\delta\hat{S}_l^{[A,B]}\delta\hat{S}_{l'}^{[A,B]}\right\rangle = \sum_{LL'} M^{-1}_{lL}\left\langle\delta\tilde{S}_L^{[A,B]}\delta\tilde{S}_{L'}^{[A,B]}\right\rangle M^{-1}_{L'l'}; \quad \left\langle\hat{S}_l^{[A,B]}\right\rangle = S_l^{[A,B]}.$$

The power spectra associated with the MFs are linear combinations of the skew spectra (see equation 3). In our approach, the power spectra associated with the MFs are secondary and can be constructed using the skew spectra that are estimated directly from the data.

No construction of an estimator is complete without an estimate of its variance. The variance or the scatter in certain situations can be computed using MC simulations which are computationally expensive. In our approach, it is possible to compute the covariance of our estimates of various S_l, that is, $\langle\delta S_l\delta S_{l'}\rangle$, under the same simplifying assumption that higher order correlation functions can be approximated as Gaussian. This allows us to express the error covariance in terms of the relevant power spectra. The generic expression can be written as

$$\left[\hat{V}_k^{(2)}\right]_l = \sum_{l'}[M^{-1}]_{ll'}\left[\tilde{V}_k^{(2)}\right]_l; \qquad \left\langle\delta\hat{V}_k^{(2)}\delta\hat{V}_{k'}^{(2)}\right\rangle = \sum_{LL'} M^{-1}_{lL}\left\langle\delta\left[\tilde{V}_k^{(2)}\right]_l\delta\left[\tilde{V}_{k'}^{(2)}\right]_{l'}\right\rangle M^{-1}_{L'l'}. \tag{45}$$

Here, we would like to point out that, in case of limited sky coverage, it may not be possible to estimate the skew spectra mode by mode as the mode-coupling matrix may become singular and a broad binning of the specra may be required. In the limit of near-all-sky coverage and isotropic noise, the expressions for the scatter take relatively simpler forms:

$$\left\langle\delta S_l^{[X,Y]}\delta S_{l'}^{[X,Y]}\right\rangle = f_{\rm sky}^{-1}\frac{2}{2l+1}\left[\mathcal{C}_l^{[X,X]}\mathcal{C}_{l'}^{[Y,Y]} + \left(S_l^{[X,Y]}\right)^2\right]\delta_{ll'}; \qquad \{X,Y\} \in \{\kappa, \kappa^2, \nabla\kappa(\hat{\boldsymbol{\Omega}})\cdot\nabla\kappa(\hat{\boldsymbol{\Omega}}), \nabla^2\kappa(\hat{\boldsymbol{\Omega}})\}. \tag{46}$$

Here the fraction of sky covered by the survey is denoted by $f_{\rm sky}$. The expressions for the skew spectra $S_l^{[\kappa^2,\kappa]}$, $S_l^{[\kappa^2,\nabla^2\kappa]}$and $S_l^{[\nabla\kappa\cdot\nabla\kappa,\nabla^2\kappa]}$ are given in equations (14)–(16). The expressions for covariance also depend on a set of power spectra, that is, $S_l^{[\kappa^2,\kappa^2]}$, $S_l^{[\nabla^2\kappa,\nabla^2\kappa]}$, $S_l^{[\nabla\kappa\cdot\nabla\kappa,\nabla^2\kappa]}$ and $\mathcal{C}_l^{\kappa,\kappa}$. These are given by the following expressions:

$$\mathcal{C}_l^{\nabla\cdot\nabla,\nabla\cdot\nabla} = \sum_{l'l''}(\mathcal{C}_{l'}+N_{l'})(\mathcal{C}_{l''}+N_{l''})[l_1(l_1+1)+l_2(l_2+1)-l(l+1)]^2 I^2_{ll'l''}W_{l'}W_{l''}; \tag{47}$$

$$\mathcal{C}_l^{[\kappa^2,\kappa^2]} = \sum_{l'l''}(\mathcal{C}_{l'}+N_{l'})(\mathcal{C}_{l''}+N_{l''})I^2_{ll'l''}W_{l'}W_{l''}; \quad \mathcal{C}_l^{[\nabla^2\kappa,\nabla^2\kappa]} = l^2(l+1)^2(\mathcal{C}_l+N_l)W_l\,. \tag{48}$$

Here $\mathcal{C}_l$ is the ordinary 'theoretical' convergence power spectrum defined in equation (12) which includes noise, that is, $\mathcal{C}_l W_l$ is replaced with $\mathcal{C}_l W_l + N_l$ with $N_l = 4\pi\sigma_{\rm i}^2/N_{\rm gal}$. Here $\sigma_{\rm i}$ is the intrinsic ellipticity distribution of galaxies and $N_{\rm gal}$ is the number of galaxies per arcmin^2. Using these equations, it is possible to compute the scatter in various skew spectra. These results can also be extended to take into account the cross-correlation between various skew spectra extracted from the same data. Using a less compact notation, we can write

$$\left\langle\delta S_l^{[\kappa^2,\kappa]}\delta S_l^{[\kappa^2,\kappa]}\right\rangle = f_{\rm sky}^{-1}\frac{1}{2l+1}\left[\mathcal{C}_l^{[\kappa^2,\kappa^2]}\mathcal{C}_l^{[\kappa,\kappa]} + \left(S_l^{[\kappa^2,\kappa]}\right)^2\right]; \tag{49}$$

$$\left\langle\delta S_l^{[\kappa^2,\nabla^2\kappa]}\delta S_l^{[\kappa^2,\nabla^2\kappa]}\right\rangle = f_{\rm sky}^{-1}\frac{1}{2l+1}\left[\mathcal{C}_l^{[\kappa^2,\kappa^2]}\mathcal{C}_l^{[\nabla\cdot\nabla,\nabla\cdot\nabla]} + \left(S_l^{[\kappa^2,\nabla^2\kappa]}\right)^2\right]; \tag{50}$$

$$\left\langle\delta S_l^{[\nabla\kappa\cdot\nabla\kappa,\nabla^2\kappa]}\delta S_l^{[\nabla\kappa\cdot\nabla\kappa,\nabla^2\kappa]}\right\rangle = f_{\rm sky}^{-1}\frac{1}{2l+1}\left[\mathcal{C}_l^{[\nabla^2\kappa,\nabla^2\kappa]}\mathcal{C}_l^{[\nabla\cdot\nabla,\nabla\cdot\nabla]} + \left(S_l^{[\nabla\kappa\cdot\nabla\kappa,\nabla^2\kappa]}\right)^2\right]. \tag{51}$$

The cumulative signal-to-noise ratio up to a given $l_{\rm max}$, using these expressions, for estimators $S^{(0)}$ can now be expressed as

$$\left[\left(\frac{S}{N}\right)^0_{\rm lmax}\right]^2 = f_{\rm sky}\sum_l^{l_{\rm max}}(2l+1)\left\{\frac{\left(S_l^{[\kappa^2,\kappa]}\right)^2}{\left[\mathcal{C}_l^{[\kappa^2,\kappa^2]}\mathcal{C}_l^{[\kappa,\kappa]} + \left(S_l^{[\kappa^2,\kappa]}\right)^2\right]}\right\}. \tag{52}$$

The S/N for the other two estimators $S^{(1)}$ and $S^{(2)}$ can be defined likewise. The different skew spectra that we have studied here are not completely independent. Their covariance can be analysed using the same procedure, allowing their joint estimation from a single data set:

$$\left\langle\delta S_l^{[\kappa^2,\kappa]}\delta S_l^{[\kappa^2,\nabla^2\kappa]}\right\rangle = f_{\rm sky}^{-1}\frac{1}{2l+1}\left(\mathcal{C}_l^{[\kappa^2,\kappa^2]}\mathcal{C}_l^{[\kappa,\nabla^2\kappa]} + S_l^{[\kappa^2,\nabla^2\kappa]}S_l^{[\kappa,\kappa^2]}\right); \tag{53}$$

$$\left\langle\delta S_l^{[\kappa^2,\kappa]}\delta S_l^{[\nabla\kappa\cdot\nabla\kappa,\nabla^2\kappa]}\right\rangle = f_{\rm sky}^{-1}\frac{1}{2l+1}\left(S_l^{[\kappa^2,\nabla^2\kappa]}\mathcal{C}_l^{[\kappa,\nabla\kappa\cdot\nabla\kappa]} + \mathcal{C}_l^{[\kappa^2,\nabla\kappa\cdot\nabla\kappa]}\mathcal{C}_l^{[\kappa,\nabla^2\kappa]}\right); \tag{54}$$

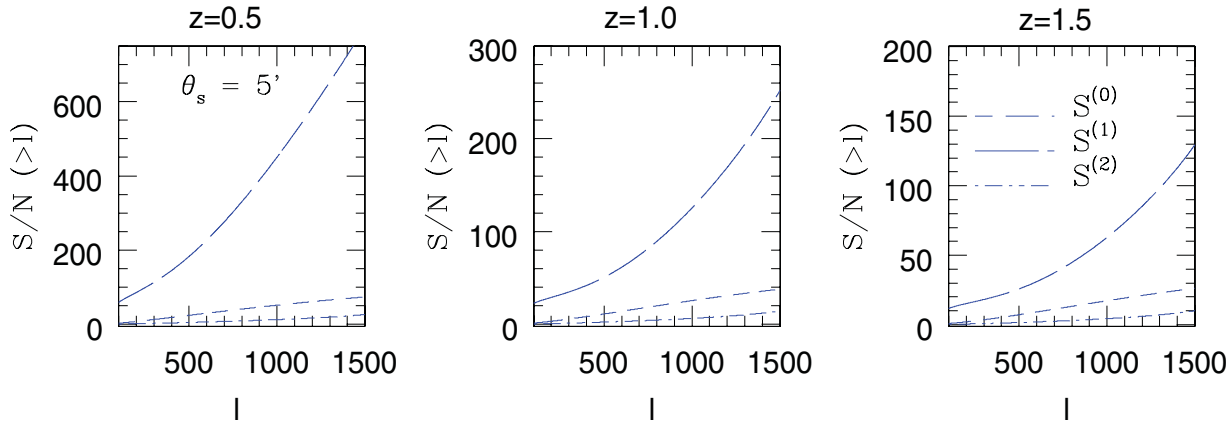

Figure 11. The cumulative *S/N* values ($> l$) associated with the *gravity-induced* skew spectra for $S_l^{(0)}$, $S_l^{(1)}$ and $S_l^{(2)}$ are plotted as a function of the wavenumber l. We have assumed a full-sky coverage, $f_{\rm sky} = 1$. The results plotted are for $l_{\rm max} = 4000$ and the smoothing angular scale is $\theta_{\rm s} = 5$. The curves from the top to bottom are $S_l^{(1)}$, $S_l^{(0)}$ and $S_l^{(2)}$, respectively. The *S/N* is highest for $S^{(1)}$. The non-Gaussianity decreases with the increase in source redshift. However, the power spectrum and hence the scatter increases with redshift. This makes it easier to probe non-Gaussianity at relatively lower redshifts.

$$\left\langle \delta S_l^{[\kappa^2,\nabla^2\kappa]} \delta S_l^{[\nabla\kappa\cdot\nabla\kappa,\nabla^2\kappa]} \right\rangle = f_{\rm sky}^{-1} \frac{1}{2l+1} \left(\mathcal{C}_l^{[\kappa^2,\nabla\kappa\cdot\nabla\kappa]} \mathcal{C}_l^{[\nabla^2\kappa,\nabla^2\kappa]} + S_l^{[\kappa^2,\nabla^2\kappa]} S_l^{[\nabla^2\kappa,\nabla\kappa\cdot\nabla\kappa]} \right). \tag{55}$$

The above results can be generalized to compute the cross-covariance of S_l from different sources of bispectrum. The following quantities are required to compute the necessary cross-covariances:

$$\mathcal{C}_l^{[\kappa,\nabla^2\kappa]} = -l(l+1)\mathcal{C}_l; \quad \mathcal{C}_l^{[\kappa^2,\nabla\kappa\cdot\nabla\kappa]} = \sum_{l'l''} (\mathcal{C}_{l'} W_{l'} + N_l)(\mathcal{C}_{l''} W_{l''} + N_{l''}) I^2_{ll'l''} [l'(l'+1) + l''(l''+1) - l(l+1)]; \tag{56}$$

$$\mathcal{C}_l^{[\kappa,\nabla\kappa\cdot\nabla\kappa]} = -\sum_{l'l''} [l'(l'+1) + l''(l''+1) - l(l+1)] \mathcal{B}_{ll'l''} J_{ll'l''} W_{l'} W_{l''}. \tag{57}$$

We have discussed the lowest order departure from Gaussianity in MFs using a third-order statistic, namely, the bispectrum. The next-to-leading descriptions are characterized by the trispectrum which is a fourth-order statistic. It is possible to extend the definition of skew spectra to the case of kurt spectra or the power spectrum associated with trispectra. The power spectra associated with the MFs can be defined completely up to fourth order using the skew and kurt spectra. However, the corrections to leading-order statistics from kurt spectra are subdominant and leading-order terms are consequently sufficient to study the departure from Gaussianity. In any case, it is nevertheless straightforward to implement an estimator which will estimate the power spectrum associated with the MFs from noisy data by including both third-order and fourth-order statistics; this issue has been dealt with in detail in Munshi et al. (2010) in the context of CMB sky. The same results will also be applicable for weak-lensing surveys.

In addition to the three genralized skew spectra that define the MFs at lowest order in non-Gaussianity, it is indeed possible to construct additional skew spectra that work with different sets of weights. In principle, an arbitrary number of such skew spectra can be constructed though they will not have direct links with the morphological properties that we have focused on. In this paper, they can still be used as a source of independent information on the bispectrum and can be used, in principle, to separate sources of non-Gaussianity, whether primordial or gravity induced. The cumulative *S/N* of detection for the gravity-induced non-Gaussianity is depicted as a function of resolution in Figs 11 and 12 for three different source redshifts $z_{\rm s} = 0.5$, 1.0 and 1.5. In Fig. 11, an ideal all-sky noise-free experiment is considered, whereas Fig. 12 includes (Gaussian) noise due to intrinsic ellipticity distribution of source galaxies.

7 NEXT-TO-LEADING-ORDER CORRECTIONS TO THE MINKOWSKI FUNCTIONALS FROM THE TRISPECTRUM

The skew spectra $S_l^{(i)}$ and the related skewness parameters $S^{(i)}$ completely specify the MFs at leading order. The next-to-leading-order corrections are determined by a set of four kurtosis parameters $K^{(i)}$ (Munshi et al. 2011b). These generalized kurtosis parameters are constructed from the trispectrum using varying weights to sample different modes. This method is very similar to construction of the generalized skew spectra and their associated skewness parameters from the bispectrum described in previous sections. The kurt spectra are constructed by cross-correlating maps that are constructed from original maps and combination of maps constructed from the original map, for example, $\nabla\Phi(\hat{\boldsymbol{\Omega}})$ and $\nabla^2\Phi(\hat{\boldsymbol{\Omega}})$. The four kurtosis parameters are natural generalizations of the ordinary kurtosis $K^{(0)}$ and can most easily be estimated in real space. The normalization of these kurtosis parameters is determined by suitable combinations of powers of the parameters σ_0 and σ_1 (Matsubara 2010):

$$K^{(0)} \equiv \frac{1}{\sigma_0^6} K^{(\kappa^4)} = \frac{\langle \kappa^4(\hat{\boldsymbol{\Omega}}) \rangle_{\rm c}}{\sigma_0^6}; \quad K^{(1)} \equiv \frac{1}{\sigma_0^4 \sigma_1^2} K^{(\kappa^3\nabla^2\kappa)} = \frac{\langle \kappa^3(\hat{\boldsymbol{\Omega}}) \nabla^2\kappa(\hat{\boldsymbol{\Omega}}) \rangle_{\rm c}}{\sigma_0^4 \sigma_1^2}; \tag{58}$$

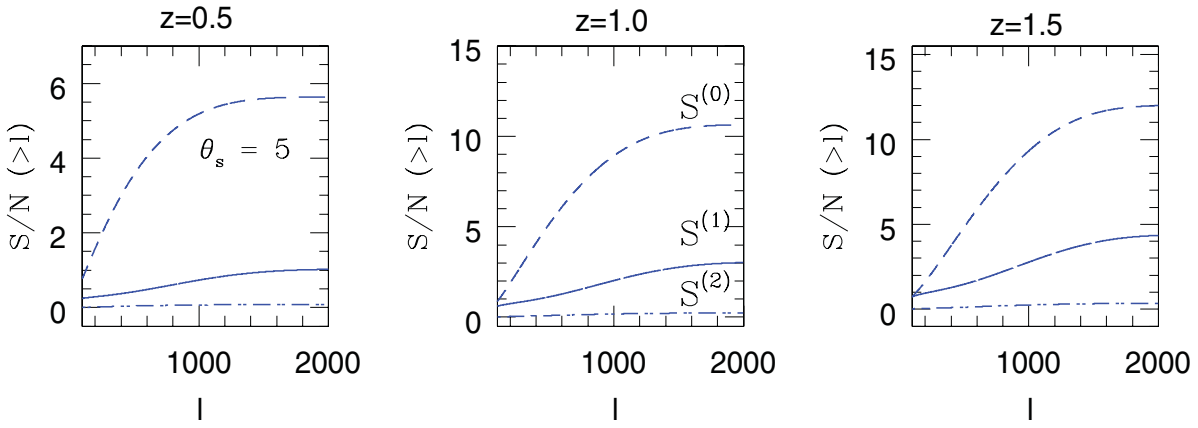

Figure 12. Same as the previous figure, but noise due to the inclusion of the intrinsic ellipticity distribution in the computation of scatter.

$$K^{(2)} \equiv K^{(2a)} + K^{(2b)} \equiv \frac{1}{\sigma_0^2\sigma_1^4} K^{(\kappa|\nabla\kappa|^2\nabla^2\kappa)} + \frac{1}{\sigma_0^2\sigma_1^4} K^{(|\nabla\kappa|^4)} = \frac{\langle\kappa|[\nabla\kappa(\hat{\mathbf{\Omega}})]|^2[\nabla^2\kappa(\hat{\mathbf{\Omega}})]\rangle_{\rm c}}{\sigma_0^2\sigma_1^4} + \frac{\langle|(\nabla\kappa)|^4\rangle_{\rm c}}{\sigma_0^2\sigma_1^4}; \tag{59}$$

$$K^{(3)} \equiv \frac{1}{2\sigma_0^2\sigma_1^4} K^{(|\nabla\kappa|^4)} = \frac{\langle|\nabla\kappa(\hat{\mathbf{\Omega}})|^4\rangle_{\rm c}}{2\sigma_0^2\sigma_1^4}, \quad \text{where} \quad |\nabla\kappa(\hat{\mathbf{\Omega}})|^2 = \nabla\kappa(\hat{\mathbf{\Omega}})\cdot\nabla\kappa(\hat{\mathbf{\Omega}}). \tag{60}$$

Unlike the skewness parameters, the kurtosis parameters also get contributions from Gaussian (unconnected) components. The subscript 'c' above, however, refers to the non-Gaussian or the connected part of the contribution which is directly liked to the trispectrum. The correction to the MFs $\delta V^{(i)}(\nu)$ as defined in equation (3) from the next-to-leading-order terms consists of both the Kurtosis parameters $K^{(i)}$ and the product of two skewness parameters $S^{(i)}$ (Matsubara 2010):

$$\delta V_0^{(4)}(\nu) = \frac{[S^{(0)}]^2}{72} H_5(\nu) + \frac{K^{(0)}}{24} H_3(\nu); \tag{61}$$

$$\begin{aligned}
\delta V_1^{(4)}(\nu) &= \frac{[S^{(0)}]^2}{72} H_6(\nu) + \left[\frac{K^{(0)} - S^{(0)}S^{(1)}}{24}\right] H_4(\nu) - \frac{1}{12}\left\{K_1 + \frac{3}{8}[S^{(1)}]^2\right\} H_2(\nu) - \frac{1}{8}K^{(3)};\\
\delta V_2^{(4)}(\nu) &= \frac{[S^{(0)}]^2}{72} H_7(\nu) + \left[\frac{K^{(0)} - S^{(0)}S^{(1)}}{24}\right] H_5(\nu) - \frac{1}{6}\left[K^{(1)} + \frac{1}{2}S^{(0)}S^{(2)}\right] H_3(\nu) - \frac{1}{2}\left[K^{(2)} + \frac{1}{2}S^{(1)}S^{(2)}\right] H_1(\nu).
\end{aligned} \tag{62}$$

The analytical modelling of four-point correlation functions is most naturally done in the harmonic domain. They are described by the angular trispectrum $\mathcal{T}^{l_1l_2}_{l_3l_4}(L)$ which is defined through the relation $\langle\kappa_{l_1m_1}\kappa_{l_2m_2}\kappa_{l_3m_3}\kappa_{l_4m_4}\rangle_{\rm c} = \sum_L I_{l_1l_2L} I_{l_3l_4L} \mathcal{T}^{l_1l_2}_{l_3l_4}(L)$. The trispectrum $\mathcal{T}^{l_1l_2}_{l_3l_4}(l)$ is expressed in terms of the reduced trispectrum $P^{l_1l_2}_{l_3l_4}(l)$. The following expression was introduced by Hu (2000, 2001) and Hu & Okamoto (2002) and encodes all possible inherent symmetries:

$$\mathcal{T}^{l_1l_2}_{l_3l_4}(l) = P^{l_1l_2}_{l_3l_4}(l) + (2l+1)\left[\sum_{l'}(-1)^{l_2+l_3}\begin{Bmatrix} l_1 & l_2 & l \\ l_4 & l_3 & l' \end{Bmatrix} P^{l_1l_3}_{l_2l_4}(l') + \sum_{l'}(-1)^{L+L'}\begin{Bmatrix} l_1 & l_2 & l \\ l_3 & l_4 & l' \end{Bmatrix} P^{l_1l_4}_{l_3l_2}(l')\right]. \tag{63}$$

The matrices in curly brackets represent 6j symbols which are defined using 3j symbols [see Edmonds (1968) for more detailed discussions]. The entities $P^{l_1l_2}_{l_3l_4}(l)$ can be further decomposed into terms of the *reduced* trispectrum $\tau^{l_1l_2}_{l_3l_4}(l)$. A specific model for the non-Gaussianity – either primordial or gravity induced – has a specific prescription for the reduced trispectrum which in turn describes the next-to-leading-order corrections to the MFs:

$$P^{l_1l_2}_{l_3l_4}(l) = \tau^{l_1l_2}_{l_3l_4}(l) + (-1)^{\Sigma_U}\tau^{l_2l_1}_{l_3l_4}(l) + (-1)^{\Sigma_L}\tau^{l_1l_2}_{l_4l_3}(l) + (-1)^{\Sigma_L+\Sigma_U}\tau^{l_2l_1}_{l_4l_3}(l); \quad \Sigma_L = l_1+l_2+l; \quad \Sigma_U = l_3+l_4+l. \tag{64}$$

In addition to the original convergence trispectra $[\mathcal{T}^{(0)}]$ generally used in the literature, we can define a set of four trispectra which use different weights to samples of modes defined by the quadruplet of harmonic numbers l_i:

$$[\mathcal{T}^{(0)}]^{l_1l_2}_{l_3l_4}(l) = \mathcal{T}^{l_1l_2}_{l_3l_4}(l); \quad [T^{(1)}]^{l_1l_2}_{l_3l_4}(l) = \frac{1}{4}\left[l_1(l_1+1) + l_2(l_2+1) + l_3(l_3+1) + l_4(l_4+1)\right]\mathcal{T}^{l_1l_2}_{l_3l_4}(l); \tag{65}$$

$$[\mathcal{T}^{(2)}]^{l_1l_2}_{l_3l_4}(l) = \frac{1}{4}\left\{l(l+1) - [l_1(l_1+1) + l_2(l_2+1)][l_3(l_3+1) + l_4(l_4+1)]\right\}\mathcal{T}^{l_1l_2}_{l_3l_4}(l); \tag{66}$$

$$[\mathcal{T}^{(3)}]^{l_1l_2}_{l_3l_4}(l) = \frac{1}{4}\left\{[l_1(l_1+1) + l_2(l_2+1) - l(l+1)][l_3(l_3+1) + l_4(l_4+1) - l(l+1)]\right\}\mathcal{T}^{l_1l_2}_{l_3l_4}(l). \tag{67}$$

The power spectrum associated with these kurtosis parameters, that is, the kurt spectrum, is defined in terms of the trispectrum, extending the previously defined skew spectra along fairly obvious lines. The estimation of these kurt spectra would be done by cross-correlating relevant

fields used to construct the related kurtosis in real space $K^{(i)}$:

$$K^{(i)} = \sum_{l_i} \sum_{L} [\mathcal{T}^{(i)}]^{l_1 l_2}_{l_3 l_4}(L) I_{l_1 l_2 L} I_{l_3 l_4 L}; \quad K^{(i)}_l = \sum_{l_i} [\mathcal{T}^{(i)}]^{l_1 l_2}_{l_3 l_4}(l) J_{l_1 l_2 l} J_{l_3 l_4 l}; \quad \sum_i (2l+1) K^{(i)}_l = K^{(i)}. \tag{68}$$

The error and covariance associated with these kurt spectra can be computed using exactly the same formalism as we described in the context of estimation of skew spectra. The kurt spectra being power spectra will contain more information compared to the kurtosis which is a one-point estimator. Though one may be interested, in principle, to extract the entire trispectrum, it may be more realistic to use the kurt spectra because of the likely low *S/N* associated with individual harmonic modes.

To compute the kurtosis, one needs a reasonable model to compute the trispectra for the convergence field. This is typically done using the paraphernalia of the halo model we introduced before. The modelling of the gravity-induced trispectrum in the halo model follows the same principle as before. It involves terms from one-, two-, three- and four-halo contributions and the total can be written as

$$T_\delta(k_1, k_2, k_3, k_4) = T^{1\mathrm{h}}_\delta(k_1, k_2, k_3, k_4) + T^{2\mathrm{h}}_\delta(k_1, k_2, k_3, k_4) + T^{3\mathrm{h}}_\delta(k_1, k_2, k_3, k_4) + T^{4\mathrm{h}}_\delta(k_1, k_2, k_3, k_4). \tag{69}$$

The expressions for various contributions are listed below. These can be expressed in terms of $I^\beta_\mu(k_1, k_2, \ldots, k_\mu; z)$ defined above. Note that the two-halo term has two contributions. In the case of the one represented by $T^{2\mathrm{h}}_{31}$, there are three points in the first halo and one in the second, whereas $T^{2\mathrm{h}}_{22}$ represents two points in each halo:

$$T^{1\mathrm{h}}_\delta = I^0_4(k_1, k_2, k_3, k_4); \tag{70}$$

$$T^{2\mathrm{h}}_\delta = T^{31} + T^{22}; \qquad T^{2\mathrm{h}}_{31} = P^\delta_{\mathrm{lin}}(k_1) I^1_3(k_2, k_3, k_4) I^1_1(k_1) + \text{cyclic permutation}; \quad T^{2\mathrm{h}}_{22} = P^\delta_{\mathrm{lin}}(k_1 2) I^1_2(k_1, k_2) I^1_2(k_3, k_4) + \text{cyclic permutation}; \tag{71}$$

$$T^{3\mathrm{h}}_\delta = B^\delta_{\mathrm{lin}}(k_1, k_2, k_3) I^1_2(k_3, k_4) I^1_1(k_1) I^1_1(k_2) + P^\delta_{\mathrm{lin}}(k_1) P^\delta_{\mathrm{lin}}(k_2) I^2_2(k_3, k_4) I^1(k_1) I^1_1(k_2) + \text{cyclic permutation}; \tag{72}$$

$$T^{4\mathrm{h}}_\delta = I^1_1(k_1) I^1_1(k_2) I^1_1(k_3) I^1_1(k_4) T^\delta_{\mathrm{lin}}(k_1, k_2, k_3, k_4) + I^2_2(k_4) I^1_1(k_1) I^1_1(k_2) I^1_1(k_3) + \text{cyclic permutation}. \tag{73}$$

Here P^δ_{lin} is the linear power spectrum for the density contrast δ and $B^\delta_{\mathrm{lin}}(k_1, k_2, k_3)$, and $T^\delta_{\mathrm{lin}}(k_1, k_2, k_3, k_4)$ are the tree-level expressions for the bispectrum and trispectrum in the quasi-linear regime, respectively. The general expression for $I^\mu(k_1, k_2, \ldots, k_\mu; z)$ is given in equation (32). Detailed derivations and discussions of these expressions can be found in, for example, Cooray (2001b) and Cooray & Seth (2002). Extension of perturbative approaches can also be employed for the computation of the gravity-induced trispectrum. The accuracy of any analytical modelling is more difficult for the higher order multispectra and depends by and large on more inputs from numerical simulations. The projected tripsectrum or the convergence trispectrum $\mathcal{T}^{l_1 l_2}_{l_3 l_4}(l)$ can be expressed in terms of the underlying mass trispectrum $T^{l_1 l_2}_{l_3 l_4}(l)$ as

$$\mathcal{T}^{l_1 l_2}_{l_3 l_4}(l) = I_{l_1 l_2 l} I_{l_3 l_4 l} \int_0^{r_\mathrm{s}} \mathrm{d}r \frac{w^4(r, r_\mathrm{s})}{d^6_\mathrm{A}(r)} T^\delta \left(\frac{l_1}{d_\mathrm{A}(r)}, \frac{l_2}{d_\mathrm{A}(r)}, \frac{l_3}{d_\mathrm{A}(r)}, \frac{l_4}{d_\mathrm{A}(r)} \right). \tag{74}$$

The trispectrum for primordial non-Gaussianity exists in the literature for the local model. The results presented here clearly are generic and can be deployed to analyse arbitrary models. It is worth mentioning here that while modelling of trispectrum is relevant for the computation of corrections to the leading-order terms, they are also important in modelling the scatter in the computation of the ordinary power spectrum. Hence, the errors in σ_0 and σ_1, for example, will involve the one-point kurtosis parameters $K^{(i)}$ if contributions from non-Gaussianity are taken into account. The correlation functions that represent these kurt spectra in real space are constructed using derivative operators on the original convergence map and can be useful for surveys with smaller sky coverage:

$$K^{(0)}(\hat{\mathbf{\Omega}}_1, \hat{\mathbf{\Omega}}_2) \equiv \langle \kappa^2(\hat{\mathbf{\Omega}}_1) \kappa^2(\hat{\mathbf{\Omega}}_2) \rangle_\mathrm{c}; \quad K^{(1)}(\hat{\mathbf{\Omega}}_1, \hat{\mathbf{\Omega}}_2) \equiv \langle \kappa^2(\hat{\mathbf{\Omega}}_1) [\kappa(\hat{\mathbf{\Omega}}_2) \nabla^2 \kappa(\hat{\mathbf{\Omega}}_2)] \rangle_\mathrm{c}; \tag{75}$$

$$K^{(2)}(\hat{\mathbf{\Omega}}_1, \hat{\mathbf{\Omega}}_2) \equiv \langle \nabla\kappa(\hat{\mathbf{\Omega}}_1) \cdot \nabla\kappa(\hat{\mathbf{\Omega}}_1) [\kappa(\hat{\mathbf{\Omega}}_2) \nabla^2 \kappa(\hat{\mathbf{\Omega}}_2)] \rangle_\mathrm{c}; \quad K^{(3)}(\hat{\mathbf{\Omega}}_1, \hat{\mathbf{\Omega}}_2) \equiv \langle \nabla\kappa(\hat{\mathbf{\Omega}}_1) \cdot \nabla\kappa(\hat{\mathbf{\Omega}}_1) [\nabla\kappa(\hat{\mathbf{\Omega}}_2) \cdot \nabla\kappa(\hat{\mathbf{\Omega}}_2)] \rangle_\mathrm{c}. \tag{76}$$

These correlation functions can be computed directly in real space without any harmonic decomposition.

8 CONCLUSIONS

Weak-lensing observations offer the potential to probe the cosmological density distribution in an unbiased way. Since the angular scales probed by weak lensing are sensitive to non-Gaussianity, primarily that generated by gravitational clustering, this technique offers us the chance to push our understanding of the statistical properties of the cosmological matter field far beyond current limits.

The statistical characterization of gravitational clustering is most often performed using a hierarchy of higher order correlation functions or their collapsed counterparts which correspond to the moments of the convergence field κ. However, it is well known that non-Gaussianity can also modify the morphological properties characterized by the MFs of the relevant field κ. The MFs therefore encode information about the non-Gaussianity and can be used as an estimator. At leading order, the MFs depend on three generalized skewness parameters, S^0, S^1 and S^2. These parameters are one-point statistics constructed from the bispectrum $B_{l_1 l_2 l_3}$ using different weights for individual modes. We have generalized these one-point estimators to a set of power spectra, namely, S^0_l, $S^1{}_l$ and S^2_l. We studied how they can be expressed in terms of the bispectrum $B_{l_1 l_2 l_3}$. In real space, these power spectra are related to the relevant correlation function (equation 23). Though the correlation functions associated with the skew spectra are two-point statistics in terms of spatial order, they actually are of third (lowest) order in terms of non-Gaussianity. Hence, they carry information about the bispectrum. These statistics are in fact known as the *cumulant correlators* and the first of these statistics, $S^{(0)}$, is already well studied in the literature. The expression for a generic cumulant correlator of order $p + q$ is

$\langle \kappa^p(\hat{\mathbf{\Omega}}_1)\, \kappa^q(\hat{\mathbf{\Omega}}_2)\rangle$. It probes multispectra of order $p + q$ and is known to be related with the bias associated with overdense objects in 3D or *hotspots* in 2D (Munshi 2000).

The skewness parameters define the leading-order terms to the MFs. The next-to-leading-order terms are associated with the convergence trispectrum. The convergence trispectrum in turn is expressed in terms of the trispectrum of the projected density field. The generalized kurtosis parameters and their related power spectra can likewise be constructed from the convergence trispectra. The corresponding representations in the Fourier domain are named as the kurt spectra. We have not considered these kurt spectra in our analysis as they are subdominant, but they can be taken into account using the same formalism if required.

We have shown that the MFs can be decomposed into three different power spectra and that these power spectra can be constructed from an equal number of skew spectra that carry information completely equivalent to the original MFs at the lowest order. These power spectra in real space will correspond to correlation functions of fields that are constructed from products of various derivative fields. These spatial derivative fields are in turn constructed from the original convergence maps $\kappa(\theta_s)$. These generalized skew spectra are therefore related to the generalized cumulant correlators defined in real space. Each of these skewness parameters can be constructed from the relevant skew spectra. However, the skew spectra have the greater power in distinguishing different sources of non-Gaussianity. This is related to the fact that individual sources of non-Gaussiantity will lead to specific shapes for the skew spectra that can be tested against the observed data. We have shown that recovery of these skew spectra from noisy data in the presence of a mask is relatively straightforward. The scatter in these statistics can be estimated under certain simplifying approximations.

In this paper, we have initiated a systematic study of these skew spectra in the context of weak-lensing surveys. We have studied how the skew spectra depend on specific choices of non-linearity that include gravity-induced non-Gaussianity or primordial non-Gaussianity. We have also pointed out that the departure of MFs from Gaussianity is determined by the generalized skew spectra which are largely independent of cosmology but which depend primarily on specific models of primordial non-Gaussianity. The overall amplitudes are determined by the background cosmology as they are determined by the power spectrum of convergence. Such a clear distinction promises to help enormously in separating the non-Gaussianity, independent of cosmology.

The formalism we have developed here for the study of non-Gaussianity depends on the well-known pseudo-C_l approach for power spectrum estimation. In this approach, the effect of any mask and noise can be dealt with in a natural manner. This is achieved using a matrix that encodes mode–mode coupling. We generalized this approach to the context of generalized skew spectra and showed that the error and their covariance can also be constructed in this approach. We also performed a detailed analysis of error characteristics. The analytical characterization of errors means costly, numerical MC simulations are no longer needed and is a further strength of this approach.

It is also worth pointing out that although we have considered three generalized skew spectra which are related to the MFs, it is clearly the case that infinitely many such generalized skew spectra can be constructed with arbitrary associated weights that are *not* directly related to MFs. However, these generalized skew spectra can be analysed jointly to maximize the extraction of information.

One fly in the ointment is that we do not have a complete analytical picture of gravitational clustering. However, a number of variants of perturbative techniques which also rely on inputs from numerical simulations are widely in use. We are also reasonably confident that the halo model is capable of capturing basic features of gravitational instability. We have used these approximations to construct corresponding theoretical predictions for the skew spectra. We study them as a function of the redshift of sources as well as a smoothing function to check how sensitive the results are to various assumptions about the input physics.

Non-Gaussianity induced by gravity may be the primary source of non-Gaussianity for weak-lensing probes, but recent CMB studies have also pointed to the possibility of non-zero primordial non-Gaussianity. It is well accepted that CMB studies may be the cleanest probes to primordial non-Gaussianity. Nevertheless, LSS probes are known to reach comparable accuracy. It is therefore interesting to see if weak-lensing observations too can be used to detect and study various models of primordial non-Gaussianity. Motivated by the idea that the skew spectra might be valuable in this direction, we have studied to what extent the skew spectra can provide valuable information about various models of primordial non-Gaussianity. We specifically studied two different models of primordial non-Gaussianity, namely, the local model and the equilateral models of non-Gaussianity, and compared their contributions against the gravity-induced non-Gaussianity generated due to subsequent evolution as a function of redshift as well as angular harmonics.

The window function that we have considered here is top-hat window. Clearly, the results can be generalized to any other window, for example, the $M_{\rm ap}$ or Gaussian window functions that too are often used in various observational situations. However, the use of different window functions is not expected to change the overall conclusions.

We have ignored noise in weak-lensing surveys that arises from the intrinsic distribution of galaxy ellipticities. It is expected that noise arising from this will somewhat dilute the signatures from the non-Gaussianity, because it increases scatter. However, for a reasonable number density of galaxies, the noise power spectrum will overtake the convergence power spectrum beyond a harmonic mode l where saturation in S/N has already been reached and so will not likely to change the saturation value of the cumulative S/N. This is true for all of the estimators probed as they reach saturation for roughly the same value of l as shown in Fig. 12.

Weak-lensing statistics are very sensitive to the cut-off in halo mass used in the calculations. We have used haloes in the mass range of 10^3–$10^{16}\,{\rm M}_\odot$. Higher order statistics are typically determined by the high-end tail of the density distribution, that is, by regions within high-mass haloes. Selective choice of a specific mass range will clearly change the detailed result and can be incorporated in our analysis. The three different skew spectra that we have proposed can be used to separate up to three different components of the non-Gaussianity. Additional skew spectra can be constructed which can be used for a consistency check, though they may not have any direct link to the MFs.

The results presented here are also for a single source plane, for example, $z_s = 1$, but a realistic redshift distribution of sources can easily be incorporated in our analysis.

To summarize, we find that for $f_{NL} = 1$, which specifies the primordial non-Gaussianity, the skew spectrum is typically two orders of magnitude lower than the gravity-induced non-Gaussianity. This is true for all three different models of primordial non-Gaussianity that we have probed irrespective of the source redshift. This will mean for a reasonable value of f_{NL} (say, $f_{NL} \approx 100$), the gravity-induced non-Gaussianity and primordial non-Gaussianity will make nearly-equal contributions to the various skew spectra with roughly equal *S*/*N*. The scatter does not depend on the model of non-Gaussianity and depends only on the power spectrum. Of the three skew spectra studied, we found that the highest *S*/*N* is achieved by the skew spectra $S_l^{(1)}$ followed by $S^{(0)}$. For all three redshifts we have probed, we found that $S_l^{(2)}$ has the lowest *S*/*N* and may not be detectable even with all-sky coverage.

Finally, it is worth mentioning here that although we have studied the projected or 2D morphology of LSS as probed by weak-lensing surveys, it is indeed possible to extend these results to 3D weak-lensing surveys. 3D weak-lensing surveys generalize the tomographical studies to 3D using photometric redshifts. In future, many 3D weak-lensing surveys will provide us with an unbiased picture of the dark matter distribution. Statistical descriptors will be important to quantify such 3D distribution of dark matter. The 3D morphology of the LSS has also been studied extensively using morphological descriptors applied to redshift surveys (see Seth 2006, and the references therein). The 3D morphology is far richer than the 2D descriptors considered here for the projected surveys. In 3D, there are four MFs which correspond to the surface area V_0, volume V_1, extrinsic V_3 and intrinsic curvatures V_4. These MFs are used to define various statistics that are linked to genus and percolation statistics. *Shape statistics* have also been introduced to link the MFs with the statistical analysis of shapes and are now widely used for analysing galaxy surveys and *N*-body simulations.

In future, use of photometric information of galaxies will allow mapping out the dark matter distribution using weak-lensing surveys. Such 3D weak-lensing surveys will provide us with 3D maps of the dark matter distribution that can be probed using morphological descriptors. The direct link with the bispectrum- and trispectrum-based approach developed here can be useful in studying the growth of structure under gravitational instability. It has the potential to greatly enhance the information gained by studying projected catalogues that we have presented here.

ACKNOWLEDGMENTS

DM acknowledges support from STFC standard grant ST/G002231/1 at the School of Physics and Astronomy at Cardiff University where this work was completed. LvW is supported by the NSERC and CIfAR. JS acknowledges support from NSF AST-0645427.

REFERENCES

Babich D., 2005, Phys. Rev. D, 72, 043003
Bardeen J. M., Bond J. R., Kaiser N., Szalay A. S., 1986, ApJ, 304, 15
Beacon D. J., Refregier A., Ellis R. S., 2000, MNRAS, 318, 625
Bernardeau F., Schaeffer R., 1992, A&A, 255, 1
Bernardeau F., Colombi S., Gaztanaga E., Scoccimarro R., 2002, Phys. Rep., 367, 1
Bouchet F. R., Juszkiewicz R., Colombi S. Pellat R., 1992, ApJ, 394, L5
Cabella P., Hansen F. K., Liguori M., Marinucci D., Matarrese S., Moscardini L., Vittorio N., 2006, MNRAS, 369, 819
Canavezes A. et al., 1998, MNRAS, 297, 777
Castro P. G., Heavens A. F., Kitching T. D., 2005, Phys. Rev. D, 72, 023516
Chen X., Huang M., Kachru S., Shiu G., 2007a, J. Cosmol. Astropart. Phys., 0701, 002
Chen X., Easther R., Lim E. A., 2007b, J. Cosmol. Astropart. Phys., 0706, 023
Coles P., 1988, MNRAS, 234, 509
Cooray A., 2001a, Phys. Rev. D, 64, 043516
Cooray A. R., 2001b, PhD thesis, Univ. Chicago
Cooray A., Seth R., 2002, Phys. Rep., 372, 1
Creminelli P., 2003, J. Cosmol. Astropart. Phys., 0310, 003
Creminelli P., Nicolis A., Senatore L., Tegmark M., Zaldarriaga M., 2006, J. Cosmol. Astropart. Phys., 5, 4
Creminelli P., Senatore L., Zaldarriaga M., Tegmark M., 2007a, J. Cosmol. Astropart. Phys., 0703, 005
Creminelli P., Senatore L., Zaldarriaga M., 2007b, J. Cosmol. Astropart. Phys., 3, 19
Edmonds A. R., 1968, Angular Momentum in Quantum Mechanics, 2nd edn. Princeton Univ. Press, Princeton, NJ
Eriksen H. K., Novikov D. I., Lilje P. B., Banday A. J., Gorski K. M., 2004, ApJ, 612, 64
Fry J. N., 1984, ApJ, 279, 499
Gott J. R., Melott A. L., Dickinson M., 1986, ApJ, 306, 341
Gott J. R. et al., 1989, ApJ, 340, 625
Gott J. R., Mao S., Park C., Lahav O., 1992, ApJ, 385, 26
Hadwiger H., 1959, Math. Zh., 71, 124
Heavens A. F., 1998, MNRAS, 299, 805
Heavens A. F., 2003, MNRAS, 343, 1327
Heavens A. F., Refregier A., Heymans C. E., 2000, MNRAS, 319, 649
Heavens A. F., Kitching T. D., Taylor A. N., 2006, MNRAS, 373, 105
Heavens A. F., Kitching T. D., Verde L., 2007, MNRAS, 380, 1029

Hikage C. et al., 2002, PASJ, 54, 707
Hikage C., Taruya A., Suto Y., 2003, PASJ, 55, 335
Hikage C., Komatsu E., Matsubara T., 2006, ApJ, 653, 11
Hikage C., Coles P., Grossi M., Moscardini L., Dolag K., Branchini L., Matarrese S., 2008a, MNRAS, 385, 1513
Hikage C., Matsubara T., Coles P., Liguori M., Hansen F. K., Matarrese S., 2008b, MNRAS, 389, 1439
Hivon E., Górski K. M., Netterfield C. B., Crill B. P., Prunet S., Hansen F., 2002, ApJ, 567, 2
Hu W., 1999, ApJ, 522, L21
Hu W., 2000, Phys. Rev. D, 62, 043007
Hu W., 2001, Phys. Rev. D, 64, 083005
Hu W., Okamoto T., 2002, ApJ, 574, 566
Hui L., 1999, ApJ, 519, L9
Jain B., Seljak U., 1997, ApJ, 484, 560
Jain B., Seljak U., White S., 2000, ApJ, 530, 547
Kaiser N., 1992, ApJ, 388, 272
Kaiser N., Wilson G., Luppino G. A., 2000, ApJ, preprint (astro-ph/0003338)
Kitching T. D., Heavens A. F., Verde L., Serra P., Melchiorri A., 2008, Phys. Rev. D, 77, 103008
Komatsu E. et al., 2003, ApJS, 148, 119
Komatsu E., Spergel D. N., Wandelt B. D., 2005, ApJ, 634, 14
Limber D. N., 1954, ApJ, 119, 665
Ma C.-P., Caldwell R. R., Bode P., Wang L., 1999, ApJ, 521, L1
Matsubata T., 2010, Phys. Rev. D, 81, 083505
Matsubara T., Jain B., 2001, ApJ, 552, L89
Medeiros J., Contaldi C. R., 2006, MNRAS, 367, 39
Melott A. L., 1990, Phys. Rep., 193, 1
Mo H. J., Jing Y. P., White S. D. M., 1997, MNRAS, 284, 189
Moore B. et al., 1992, MNRAS, 256, 477
Munshi D., 2000, MNRAS, 318, 145
Munshi D., Coles P., 2000, MNRAS, 313, 148
Munshi D., Coles P., 2002, MNRAS, 329, 797
Munshi D., Coles P., 2003, MNRAS, 338, 846
Munshi D., Heavens A., 2010, MNRAS, 401, 2406
Munshi D., Jain B., 2000, MNRAS, 318, 109
Munshi D., Jain B., 2001, MNRAS, 322, 107
Munshi D., Valageas P., 2005, Phil. Trans. R. Soc. A, 363, 2675
Munshi D., Bernardeau F., Melott A. L., Schaeffer R., 1999a, MNRAS, 303, 433
Munshi D., Coles P., Melott A. L., 1999b, MNRAS, 307, 387
Munshi D., Coles P., Melott A. L., 1999c, MNRAS, 310, 892
Munshi D., Melott A. L., Coles P., 1999d, MNRAS, 311, 149
Munshi D., Valageas P., Barber A. J., 2004, MNRAS, 350, 77
Munshi D., Valageas P., van Waerbeke L., Heavens A., 2008, Phys. Rep., 462, 67
Munshi D., Smidt J., Cooray A., 2010, MNRAS, submitted
Munshi D., Smidt J., Heavens A., Coles P., Cooray A., 2011a, MNRAS, 411, 2241
Munshi D., Heavens A., Cooray A., Smidt J., Coles P., Serra P., 2011b, MNRAS, 412, 1993
Natoli et al., 2010, MNRAS, 408, 1658
Navarro J., Frenk C., White S. D. M., 1996, ApJ, 462, 563
Park C. et al., 2005, ApJ, 633, 11
Peebles P. J. E., 1980, The Large Scale Structure of the Universe. Princeton Univ. Press, Princeton, NJ
Pen U.-L., Zhang T., van Waerbeke, Mellier Y., Zhang P., Dubinski J., 2003, ApJ, 592, 664
Press W. H., Schechter P., 1974, ApJ, 187, 425
Rhoads J. E., Gott J. R. I., Postman M., 1994, ApJ, 421, 1
Sato J., Takada M., Jing Y. P., Toshifumi F., 2001, ApJ, 551, L5
Schaeffer R., 1984, A&A, 134, L15
Scoccimarro R., Colombi S., Fry J. N., Frieman J. A., Hivon E., Melott A., 1998, ApJ, 496, 586
Seljak U., 2000, MNRAS, 318, 203
Semboloni E., Heyman C., van Waerbeke L., Schneider P., 2008, MNRAS, 388, 991
Seth J. V., 2006, preprint (astro-ph/0602433)
Smith K. M., Zaldarriaga M., 2006, preprint (astro-ph/0612571)
Smith K. M., Zahn O., Dore O., 2007, Phys. Rev. D, 76, 043510
Smith K. M., Senatore L., Zaldarriaga M., 2009, J. Cosmol. Astropart. Phys., 0909, 006
Szapudi I., Szalay A. S., 1993, ApJ, 408, 43
Szapudi I., Szalay A. S., 1997, ApJ, 481, L1
Takada M., Jain B., 2003, MNRAS, 344, 857
Takada M., Jain B., 2004, MNRAS, 348, 897
Takada M., White M., 2004, ApJ, 601, L1
Taruya A., Takada M., Hamana T., Kayo I., Futamase T., 2002, ApJ, 571, 638
Tomita H., 1986, Prog. Theor. Phys., 76, 952
Valageas P., 2000, A&A, 356, 771
Valageas P., Barber A. J., Munshi D., 2004, MNRAS, 347, 654

Valageas P., Munshi D., Barber A. J., 2005, MNRAS, 356, 386
van Waerbeke L. et al., 2000, A&A, 358, 30
Van Waerbeke L., Hamana T., Scoccimarro R., Colombi S., Bernardeau F., 2001, MNRAS, 322, 918
Verde L., Wang L., Heavens A., Kamionkowski M., 2000, MNRAS, 313, L141
Villumsen J. V., 1996, MNRAS, 281, 369
Wittman D., Tyson J., Kirkman D., Dell'Antonio I., Bernstein G., 2000, Nat, 405, 143
Yadav A. P. S., Wandelt B. D., 2008, Phys. Rev. Lett., 100, 181301

This paper has been typeset from a TEX/LATEX file prepared by the author.